Could the mantle have caused subsidence of the Congo Basin?

Susanne J.H. Buiter[a,b,c,*], Bernhard Steinberger[d,b,c], Sergei Medvedev[b], Joya Tetreault[a]

[a] *Geodynamics Team, Geological Survey of Norway, Leiv Eirikssons vei 39, 7491 Trondheim, Norway*
[b] *Physics of Geological Processes, University of Oslo, Sem Selands vei 24, 0316 Oslo, Norway*
[c] *Centre of Advanced Study, Drammensveien 78, 0271 Oslo, Norway*
[d] *GFZ German Research Centre for Geosciences, Helmholtzstrasse 6, 14467 Potsdam, Germany*

Abstract

The Congo Basin is characterised by a near-circular shape, a pronounced negative free-air gravity anomaly, and a subsidence history that is slow and long-lived. The basin is often considered as an intracratonic basin, implying an unknown formation mechanism. However, the Congo Basin probably initiated by Precambrian rifting and the larger part of its older subsidence history could be explained by post-rift thermal relaxation. The uppermost layer of Mesozoic to Cenozoic sedimentary rocks in the basin appears discontinuous in its evolution and several studies have proposed that these rocks were deposited in response to a process in the mantle. We have examined gravity data and seismic tomographic models to evaluate the role of the sub-crustal

*Corresponding author

Email addresses: susanne.buiter@ngu.no (Susanne J.H. Buiter), bstein@gfz-potsdam.de (Bernhard Steinberger), sergeim@fys.uio.no (Sergei Medvedev), joya.tetreault@ngu.no (Joya Tetreault)

mantle in the more recent evolution phase of the Congo Basin. Using seismic tomographic models of the upper mantle and lithospheric thickness models, we show that the Congo Basin is underlain by a thick lithosphere and that the basin boundary likely coincides with the boundary of the Congo Craton. We have reduced the EGM2008 free-air gravity field by correcting for topography and sediments. We find that the observed negative gravity anomaly is mainly due to the sedimentary units in the basin. The reduced gravity field has slightly negative to positive anomalies over the basin, depending on the densities assigned to the sedimentary rock package. We have analysed thirteen whole-mantle and five upper-mantle tomographic models and show that they do not provide supporting evidence that the sub-lithospheric mantle played a primary role in the more recent subsidence of the Congo Basin. We speculate that deposition of the Mesozoic-Cenozoic rocks could have raised the surface elevation of the Congo Basin to the present average level of ∼400 m above sea-level and that the last subsidence phase could be a consequence of the sediment load rather than the cause.

Keywords: Intracratonic basin, Tomography, Congo Basin, Congo Craton, Gravity anomalies, Mantle flow

---

1. Introduction

The Congo Basin (located in the Democratic Republic of Congo in Central Africa) is often cited as a classic example of an intracratonic sedimentary basin: it is an almost circular depression (Fig. 1a) with negative free-air gravity anomalies (Fig. 1b, d), which experienced slow subsidence over long periods of time. The upper layer of Mesozoic - Cenozoic sedimentary rocks was deposited during little tectonic activity and several studies have proposed that the subsidence that created the accommodation space for these sediments may be linked to processes below the crust (Hartley and Allen, 1994; Downey and Gurnis, 2009; Crosby et al., 2010; Forte et al., 2010). This inspired us to examine gravity data and seismic tomographic models to evaluate the role of mantle processes in causing subsidence of the Congo Basin.

The present-day Congo Basin is surrounded by topographically higher areas: the rift flanks of the Central African Rift to the north, the East African Rift to the east, the South African (Kalahari) Plateau to the south, and the Mayombe Mountains to the west. Earthquake focal mechanisms indicate a state of compressive stress, which previous studies have linked to the "background" stress field of the African plate caused by the oceanic spreading centres surrounding it or to the effect of a dynamically driven topography contrast between the basin and the East African and South African plateaus (Ayele, 2002; Delvaux and Barth, 2010; Craig et al., 2011). Unfortunately, detailed information on the basin fill is limited; only four deep wells were drilled in the Congo Basin (Samba, Dekese, Mbandaka-1 and Gilson-1, Fig. 1a) and most of the 1970's Esso/Texaco seismic survey is not publicly available. A description and interpretation of some of these data is in Lawrence and Makazu (1988), Daly et al. (1992), and Kadima et al. (2011a). The basin contains up to 9 km of sedimentary rocks of Precambrian to Tertiary age (Fig. 2b). The basin is thought to have been initiated by Neoproterozoic extension and the older, pre-Cretaceous sediments were probably deposited during a long post-rift subsidence phase (Lawrence and Makazu, 1988; Daly et al., 1992;

Crosby et al., 2010; Kadima et al., 2011b). The evolution of the basin was discontinuous and there is clear evidence for stratigraphic unconformities of Neoproterozoic, early Palaeozoic (Pan-African), and Permian-Triassic ("Hercynian") ages. The early Palaeozoic and Permian-Triassic episodes have been linked to NE-SW-oriented compressional deformation in the centre of the basin by Daly et al. (1992). However, the interpreted basement uplift (Kiri High) may be less pronounced than previously thought and the basement may instead be composed of salt-rich sediments (Kadima et al., 2011a). The two wells drilled by REMINA, Samba (1955, 2038 m) and Dekese (1956, 1856 m), mainly encountered sandstone, schists, and clay layers and did not reach basement (Cahen et al., 1959, 1960). The Mbandaka-1 (4350 m) and Gilson-1 (4665 m) wells were drilled by Esso Zaire in 1981 and reached Cambrian sedimentary units, but again not basement (Daly et al., 1992). Tectonic subsidence curves obtained by backstripping these four wells (Kadima et al., 2011b) show very slow subsidence since the Pan-African event (about 550 Ma) (see also Crosby et al. (2010), though this study assigns a younger age of 480 Ma to the Pan-African). Such slow subsidence is similar to the subsidence signal of other intracontinental basins (Xie and Heller, 2009), but the Congo curves could also be fit by subsidence curves obtained from moderate extension of a thick lithosphere (Crosby et al., 2010; Kadima et al., 2011b).

The upper, approximately 1 km-thick early Cretaceous to Quaternary sedimentary rocks were deposited in continental environments and are untilted. Several authors have pointed out that the deposition of these Mesozoic - Cenozoic sedimentary rocks does not seem to be linked to an extensional or compressional event and that it is difficult to determine the subsidence driving-mechanism that created accommodation space for deposition of these sediments (Daly et al., 1992; Giresse, 2005). Different hypotheses have been put forward:

(1) Hartley and Allen (1994) suggested that sub-crustal dense material or a downward-directed dynamic force at the base of the lithosphere could cause the subsidence that created space for deposition of the Mesozoic - Cenozoic sediments. The negative Bouguer gravity anomaly over the basin (Fig. 1c) would be the result of a combination of a negative gravity anomaly from lower density sediments in the basin with a positive anomaly from a higher density body in the sub-crustal mantle, which isostatically compensates the sediments. Using numerical models, Downey and Gurnis (2009) showed that a high-density body within the deeper lithosphere could account for the topography and negative free-air gravity data over the basin. The hypothesis of a dense lithospheric body raises a number of intriguing questions pertaining to the origin of the body, how long it existed, and if it could have caused slow subsidence over even longer periods of time.

(2) Crosby et al. (2010) and Forte et al. (2010) explained the last basin subsidence phase by downward-directed sub-lithospheric mantle flow beneath the basin driven by small plumes rising up below the basin flanks. They interpret slow velocity anomalies in the mantle to the west and east of Congo in some tomographic models (Ritsema et al., 2004; Simmons et al., 2007) as evidence to support this theory. This theory would require upward-directed mantle flow around the basin to explain the near-circular geometry and it is a hypothesis that can be tested with tomographic models by different research groups.

(3) Alternatively, the Congo Basin acquired its modern shape at ∼30 Ma through tectonic uplift of swells surrounding the basin (Burke and Gunnell, 2008). A similar scenario was suggested by Sahagian (1993) to explain the basin evolution since the Late Jurassic. Burke and Gunnell (2008) propose that the swells were created by sub-lithospheric shallow mantle convection, as in the models of England and Houseman (1984). These 2-D models of convection in the upper mantle show how surface uplift and tectonic subsidence with a wavelength of ∼2000 km may develop below a stationary plate (England and Houseman, 1984). Sedimentation from the Congo Basin area into the offshore Congo fan increased syntectonically with the uplift of the swells surrounding the basin (Leturmy et al., 2003). Anka et al. (2010) show that a palaeo-Congo River located near the present-day Congo River already supplied sediments to the Atlantic margin since the Late Cretaceous. This indicates that the basin acted as a source area earlier than ∼30 Ma, but does not eliminate the hypothesis that the Congo Basin is an uplift basin.

(4) A fourth hypothesis for the deposition of the Mesozoic - Cenozoic sedimentary rocks simply extends the post-rift phase after the Neoproterozoic extension into the Cenozoic. Several recent studies have suggested that thermal relaxation after extension of a 200 - 250 km thick lithosphere may explain the slow tectonic subsidence curves for Congo (Crosby et al., 2010; Kadima et al., 2011b) (see also Armitage and Allen, 2010). In this scenario, deposition of the Mesozoic - Cenozoic rocks would be during the last phase of a long post-rift subsidence history.

(5) Lithospheric delamination is another possibility for the process driving the recent subsidence of the Congo Basin (see also Downey et al., 2011). The

global S-wave tomographic model of Simmons et al. (2007) shows a prominent fast anomaly at a depth of ∼1000 km, possibly representing a high-density body that sank in the sub-lithospheric mantle underneath the Congo Basin. The high-density body may be a piece of lithosphere that detached from the overlying cratonic lithosphere. The delamination would have first led to an uplift signal at the surface caused by isostatic rebound, followed by subsidence caused by mantle downwelling as the detached body sinks into the mantle.

Another possibility, which we will not investigate, is that the subsidence of the Congo Basin was produced by edge-driven convection (King and Ritsema, 2000). This process would cause subsidence near the cratonic edge instead of the centre of the basin and therefore is not a viable explanation for subsidence of the Congo Basin.

In this study, we examine gravity data and tomographic models to evaluate the role of the sub-crustal mantle in the Mesozoic - Cenozoic subsidence history of the Congo Basin and differentiate between these five hypotheses. We estimate residual gravity anomalies that could be linked to density differences in the crust or mantle. We then determine the current boundaries of the Congo Craton by evaluating five lithospheric thickness models and five tomographic models of the upper mantle. Finally, we examine thirteen tomographic models of the whole mantle and five tomographic models of the upper mantle with the aim to delineate the deeper mantle structure under the Congo Basin in reference to the five testable hypotheses.

2. Gravity anomalies of the Congo Basin

The Congo Basin is characterised by negative gravity anomalies. The global EGM2008 (Pavlis et al., 2008) free-air gravity field, in particular, clearly outlines the basin (Fig. 1b-d). The EGM2008 data set is based on both terrestrial and satellite data (Pavlis et al., 2008). For the Congo Basin, the EGM2008 data (Fig. 1b) is mainly from the land gravity measurements reported in Evrard et al. (1960) (Fig. 1d) (pers. comm. Joshua Kennerly, National Geospatial-Intelligence Agency). After the topographic correction is applied to the gravity data, the Congo basin is associated with negative Bouguer anomalies (Fig. 1c), although larger negative anomalies occur to the south associated with the high elevation of southern Africa.

Hartley and Allen (1994) pointed out that the negative Bouguer anomaly is too large to be explained by density differences that exist only in the crust. They proposed that either a dense region in the (lithospheric or asthenospheric) upper mantle isostatically compensates the low-density sediments in the basin, or that a non-isostatic dynamic force acts in the downward direction at the base of the lithosphere. Recent studies have also placed the depth of isostatic compensation at different levels whithin the lithosphere or asthenosphere. Kadima et al. (2011b) showed that reducing the free-air gravity anomaly with the gravity effect of the total sediment package results in a narrow, NW-SE-oriented, positive gravity anomaly. Kadima et al. (2011b) interpret the free-air gravity field over the Congo Basin as a result of the negative effect of the sediment infill in combination with a positive anomaly due to uplift of the base of the crust. This Moho uplift would be due to the crustal thinning inherited from the Neoproterozoic rift phase which initiated the basin. The numerical models of Downey and Gurnis (2009) support the suggestion of Hartley and Allen (1994) and show that a good fit to both the negative free-air gravity and "reduced topography" data can be obtained by viscous support of a body about 1200 km wide and 100-200 km thick, with a density anomaly of 27 - 60 kg m^{-3}, at 100 km depth within the lithospheric mantle. Downey and Gurnis (2009) "reduced" topography by removing and unloading the more recent Mesozoic - Cenozoic sedimentary rocks (Fig. 2a). It is possible that compensation for the sedimentary rocks occurs deeper than 100 km in the cratonic lithosphere, assuming the cratonic root is colder, and therefore denser, than the adjacent mantle. However, the cratonic root may be unable to compensate for the low-density sedimentary rocks as suggested through isostatic balancing by Crosby et al. (2010) or because the density increase by thermal cooling is counterbalanced by a density reduction via melt extraction (Jordan, 1978). For this reason, Crosby et al. (2010) prefer a dynamic compensation mechanism by downward directed asthenospheric flow. Depending on the method used, the depth at which the low-density basin sediments are isostatically compensated can be placed at the base of the crust (Kadima et al., 2011b), a depth of 100 km within the lithosphere (Downey and Gurnis, 2009), possibly deeper in the cratonic lithosphere, or within the asthenosphere (Crosby et al., 2010).

We correct the free-air gravity field over the Congo Basin with the gravity signal of topography and the negative signal of both the upper 1 km of Mesozoic - Cenozoic rocks and the total sediment package separately, using different sediment density values. Any remaining anomalies in this reduced Bouguer gravity field must have a source in the crust or mantle below. We compute a first-order estimate of the gravity signal produced by the uppermost Mesozoic - Cenozoic sedimentary rocks (Fig. 2a,d) with a density difference of 550 kg m^{-3}. This density difference is derived by assuming the Bouguer-correction standard value of 2670 kg m^{-3} for the crust and averaging two values for the Mesozoic-Cenozoic sediment density: 2000 kg m^{-3} as used in Downey and Gurnis (2009) and 2250 kg m^{-3} as used in Kadima et al. (2011b). The gravity anomalies associated with the top layer of Mesozoic - Cenozoic rocks reach -40 mGal (Fig. 2d). Because the thickness of the Mesozoic - Cenozoic sedimentary units is minor, the resulting gravity anomaly is insensitive to a density difference of 670 (2670 - 2000) kg m^{-3} or 420 (2670 - 2250) kg m^{-3}. We compare two sediment density models in our correction for the gravity effect of the entire sediment package (from Laske and Masters, 1997) (Fig. 2b). Both sediment density models apply to the total sediment package, therefore we do not consider the Mesozoic - Cenozoic units separately. The first sediment density model assumes a sediment density of 2250 kg m^{-3} at the surface of the model (top of the Cenozoic sediments), following Kadima et al. (2011b). We assume that sediment density increases with depth, reaching 2670 kg m^{-3} at 8 km depth. This assumption is supported by basement-like density values reached in the wells (Kadima et al., 2011a). We therefore employ a density difference of 420 kg m^{-3} at the surface, linearly decreasing to 0 kg m^{-3} at 8 km depth. This implies a small density discontinuity at the basement in places where sediments are less than 8 km deep. The resulting gravity anomaly is $\sim$ -60 to -70 kg mGal (Fig. 2e). The second model also employs a linearly decreasing density difference, starting from 670 kg m^{-3} at the surface and decreasing to 0 at 8 km depth. This results in a gravity anomaly of $\sim$ -100 to -120 mGal (Fig. 2f).

Subtracting the gravity signal of the sediments from the EGM2008 Bouguer gravity field (Fig. 1c) gives a residual gravity field that has its source in the crust or mantle below the basin. Figs. 2g, h, and i show that the reduced gravity field is still associated with slightly negative values for the Congo Basin if only the Mesozoic-Cenozoic sediments are subtracted, leading to Bouguer anomalies on the order of -90 to -10 mGal. The signal changes to positive if the field is corrected for the entire sediment fill. The residual Bouguer gravity signal then varies between -40 and +20 mGal for a density difference of 420 to 0 kg m^{-3} (Fig. 2h), and between -10 to +50 mGal for a density difference of 670 to 0 kg m^{-3} (Fig. 2i).

Depending on the sediment densities used, the residual Bouguer gravity field over Congo could be slightly negative to slightly positive. This residual anomaly over the Congo Basin is surrounded by a large negative residual anomaly, indicating that the residual anomaly over the basin is more positive relative to its surroundings. In summary, we find that the negative Bouguer gravity anomaly of the Congo Basin can be largely explained by the negative gravity signal of the sediments in the basin, in agreement with the results of Kadima et al. (2011b) for the free-air gravity anomaly. The open question is at which depth these low density sediments are isostatically compensated.

3. Constraints on the Congo Craton boundaries

Considering that a relationship exists between the Congo Craton, the Congo Basin, and mantle processes below the craton, we need to characterize the composition and extent of the Congo Craton. The Congo Craton, which underlies the Congo Basin, consists of Archean and Proterozoic crust and is surrounded by Proterozoic and Pan-African fold belts (Fig. 3). It was joined with the São Francisco Craton of Brasil since the Eburnian Orogeny (2.1-1.8 Ga) (Toteu et al., 1994; De Waele et al., 2008), until they were separated when the South Atlantic opened in the Early Cretaceous (Torsvik et al., 2009). Convergence along the eastern and southern margins of the Congo Craton in the Mesoproterozoic led to the formation of the Kibaran, Irumide, and Southern Irumide Belts (De Waele et al., 2008). This convergence could have resulted from collision of island arcs and/or microcontinents and does not necessarily reflect the assembly of Congo-São Francisco with Rodinia. In fact, most studies infer that Congo-São Francisco was not part of Rodinia and only became part of Gondwana in the late Neoproterozoic-Pan-African, when it collided with Madagascar-India to the east, the Kalahari Craton to the south, and South America to the west (Meert, 2003; De Waele et al., 2008). This phase led to the formation of the Lufilian Belt to the southeast, the Damara Belt to the southwest, and the West Congo Belt to the west. Due to this long history of continental assembly and break-up, the crust and lithosphere of the Congo Craton and surroundings could have a heterogeneous composition.

Forte et al. (2010) and Crosby et al. (2010) suggest that a mantle downwelling below the craton was driven by upwelling along the craton edges. This would imply a relationship between the Congo Basin and the edges of the Congo Craton. It has also been suggested that the present-day Congo Basin could be similar to a sediment catchment area responding to uplift around the basin edges (e.g., Burke and Gunnell, 2008). Uplift could preferentially have localised along the craton edges as opposed to on the craton, as the old, thick craton would be mechanically more rigid than the surrounding regions. In addition, this type of uplift could be caused by hot mantle material which would preferentially feed into the asthenosphere surrounding the craton rather than focus under the deep craton root.

To determine if a relationship exists between processes along the craton boundaries and the basin on the craton, we first need to establish the extent of the craton itself. Unfortunately, the limits of the Congo Craton are not uniquely defined. The craton can be equated to areas older than 1 Ga, as shown in the map of crustal basement ages of Gubanov and Mooney (2009) (Fig. 3a). Alternatively, the craton could be defined as the domain in which the lithosphere is greater than a certain thickness. Below we summarise published lithospheric thickness models and tomographic studies of the upper mantle with the aim to characterise the limits of the Congo Craton from geophysical observations (Figs. 4 and 5, Table 1). Independent geochemical evidence from kimberlites and heavy minerals at two locations in the south and southeast of the Congo Craton infer a lithospheric thickness of about 200 km (Batumike et al., 2009).

In this study, we compare five lithospheric thickness models: TC1 (Artemieva, 2006), Conrad and Lithgow-Bertelloni (2006), Fishwick (2010), Pasyanos and Nyblade (2007), and Priestley et al. (2008) (Fig. 4). The global thermal model for continental lithosphere, TC1 (Artemieva, 2006), determines thermal lithospheric thicknesses from continental geotherms and the tectonic age of the basement. The large lithospheric thicknesses of the Archean kernels (Gabon, Tanzania, Angola and Zimbabwe) are quite apparent in the TC1 model (Figs. 3 and 4a), but lower thicknesses are found under the centre of the basin. The global lithospheric thickness model of Conrad and Lithgow-Bertelloni (2006) was obtained from the global tomographic model S20RTSb (Ritsema et al., 2004) by equating the maximum depth where the velocity anomaly is consistently greater than +2% to the lithosphere depth. The thickest lithosphere in the Conrad and Lithgow-Bertelloni (2006) model is directly below the Congo Basin (Fig. 4b). The African lithospheric thickness models of Fishwick (2010) and Priestley et al. (2008) were obtained by converting their tomographic models into temperature and using a geothermal gradient to derive lithospheric thickness. The Fishwick (2010) model also has the thickest lithosphere located under the basin (Fig. 4c), whereas the Priestley et al. (2008) model has high thicknesses under the basin and in the areas of the Gabon, Tanzania, and Zimbabwe cratons (Fig. 4e). The Africa lithospheric thickness model of Pasyanos and Nyblade (2007) was produced by a grid search that fits synthetic velocity profiles to average surface wave dispersion data. Like the TC1 model (Artemieva, 2006), the Pasyanos and Nyblade (2007) model also contains large values for lithospheric thickness for the Archean kernels (Gabon, Angola and Zimbabwe) (Fig. 3 and 4e). The geometric mean of these five thickness models is dominated by the values of the Gabon craton to the northwest of the basin and the Zimbabwe craton to the southeast (Fig. 4f). However, these areas also show large variability among the models (Fig. 4g). Variability between the lithospheric thickness models is expected since we are comparing results obtained with different methods and datasets. The region with lithospheric thickness values greater than 200 km in the mean model is located in the southwest part of the basin, not in the basin centre (Fig. 4h). For these five thickness models there appears to be no direct relationship between the Congo Basin and the thicker part of the Congo Craton.

Next, we compute a proxy to lithospheric thickness from five tomographic models of the upper mantle: CU_SRT1.0 (Shapiro and Ritzwoller, 2002), CU_SDT1.0 (Shapiro and Ritzwoller, 2002), KP08 (Priestley et al., 2008), LH08 (Lebedev and Van der Hilst, 2008), and SF09 (Fishwick, 2010) (Fig. 5). We follow the method of Conrad and Lithgow-Bertelloni (2006), and equate the lithospheric depth to the maximum depth where the S-wave velocity anomaly is greater than +2%. The five tomographic models of the upper mantle are, in general, sensitive to depths above 300 - 400 km and quickly loose resolution below that. Only the tomographic model from Lebedev and Van der Hilst (2008) reaches the base of the upper mantle. The tomographic models of Fishwick (2010) and Priestley et al. (2008) are specifically derived for Africa, whereas the other tomographic models (Shapiro and Ritzwoller, 2002; Lebedev and Van der Hilst, 2008) are global models. The lithospheric thickness models computed directly from the tomographic models of Fishwick (2010) and Priestley et al. (2008) show good agreement with the lithospheric thicknesses computed from tomographic data using a geothermal gradient (compare Fig. 5c with 4e, and Fig. 5e with 4c). The lithospheric thickness models computed from seismic tomographic models of the upper mantle also show variability in cratonic thickness (Fig. 5). As different seismic methods, parameterisation, and data were used to produce each tomographic model, such variations are to be expected. However, the mean model is useful to find the common features between the models. Almost all lithospheric thickness models have a thick lithosphere under the basin (Fig. 5f). The topographically higher areas surrounding the Congo Basin are located near the edges of the seismically-derived Congo Craton (Fig. 5g). Although a rigorous and accurate estimate of lithospheric thickness under the Congo Basin would require further improvement to the dataset used in the tomographic models, the level of agreement between the five tomographic models used here would suggest that a relationship between the Congo Basin and the underlying craton is possible.

4. Insights from mantle tomography

Several studies have proposed that the subsidence that created the accommodation space for the Mesozoic - Cenozoic sedimentary succession in the Congo Basin was produced by processes below the crust (Hartley and Allen, 1994; Downey and Gurnis, 2009; Crosby et al., 2010; Forte et al., 2010). We evaluate eighteen P- and S-wave tomographic models to search for seismic velocity anomalies in the mantle that could be linked to surface subsidence (Table 1). We consider both P- and S-wave models in order to have a large number of recent tomographic models which cover a broad range of methods. Mantle processes related to subsidence of the Congo Basin would have to be long-lived and therefore require relatively stationary features. Otherwise, for sinking or rising velocities between 1 to 5 cm yr^{-1} in the upper mantle and 1 to 2 cm yr^{-1} in the lower mantle (e.g., Van der Meer et al., 2010), mantle material in a depth range of 1000 km would relate to an approximate time period of 20 to 100 Ma only. We should also note that even though the African Plate is relatively stationary during our time period of interest (Burke and

Torsvik, 2004), it still experienced movement with respect to the mantle (Fig. 6). Since the Congo Basin has moved to the NE relative to the mantle over the last 200 Ma (Fig. 6), we examine a SW-NE-oriented cross-section through the tomographic models. Our second cross-section is perpendicular to this, oriented SE-NW. We search for evidence for sub-crustal anomalies below the basin, detached lithospheric material in the mantle, and asthenospheric upwellings under the basin flanks. We assume that cold material can be associated with fast seismic velocity anomalies (blue in our figures) and warm material with slow velocity anomalies (red in our figures).

Map views and cross-sections through the eighteen individual P- and S-wave tomographic models are given in Appendix A and a brief description of the models is in Table 1. Fig. 7 show map views at 200, 500, and 800 km depths, two cross-sections, and a 3-D view for a mean tomographic model and its standard deviation (CMEAN2011). The mean model is computed as an average of thirteen whole mantle, P- and S-wave tomographic models for depths below 250 km and of ten tomographic models of the whole mantle and five S-wave tomographic models of the upper mantle for depths above 250 km. In the averaging of tomographic models into CMEAN2011, the P-wave models are scaled to S-wave amplitudes using a scaling factor that assumes that the seismic anomalies are due to thermal anomalies (Steinberger and Calderwood, 2006; Steinberger and Holme, 2008). The conversion factor from relative P-wave to relative S-wave variations is depth-dependent, but stays close to 1.9 throughout the mantle. The S-wave tomographic models are converted to spherical harmonics with a 50 km depth spacing and the resulting spherical harmonic coefficients are then averaged. The mean model has a spherical harmonic degree of 63, corresponding to a half-wavelength of $\sim$318 km. It should be noted that because several of the individual models that were used in the averaging calculation have a lower horizontal resolution (Table 1), the effective resolution of the mean model will be less. A disadvantage of the averaging of tomographic models is the loss of information about the individual models, such as path coverage and inversion method. In addition, since all contributing models are weighed equally, tomographic anomalies in one model that are substantially different from the anomalies in other models may contribute significantly to the average model. This is why we also show the standard deviation of the CMEAN2011 model, which shows the differences between the contributing models. Our mean tomographic model has no potential bias towards one individual model and defines which features are common, and therefore more robust, between the models.

The map view at 200 km depth through CMEAN2011 clearly shows a high velocity anomaly below the Congo Basin, which is a reasonably robust feature among all models (Figs. 7a and A.10). This is probably the (compositional and/or thermal) anomaly resulting from the root of the Congo Craton. It will be difficult, if not impossible, to distinguish this signal of the craton from lithospheric anomalies within it, such as those suggested by Downey and Gurnis (2009). Two cross-sections through CMEAN2011 also emphasize the high velocity anomaly at lithospheric depth below the basin and show slow seismic velocity anomalies associated with the East African Rift and slow values at the base of the lower mantle (Fig. 7d, e) (see also Nyblade and Robinson, 1994). Crosby et al. (2010) suggested a mantle convective draw-down of the Congo Basin occurred in response to adjacent upwelling plumes.

One of these plumes is associated with the East African Rift and can also be seen in CMEAN2011. The elongated East African Rift correlates with a relatively N-S trending subsidence pattern, therefore additional mantle upwellings adjacent to the basin are required in order to explain the circularity of the Congo Basin. We see no indication for additional mantle upwellings in CMEAN2011 or in the separate tomographic models of the whole mantle (Figs. A.10 - A.13). The individual tomographic models of the upper mantle (CU_SRT1.0, CU_SDT1.0, KP08, LH08, SF09) show slow velocity anomalies to the north, west, and south of the basin at 200 km depth that could correlate to mantle upwellings (Fig. A.10), but there is no agreement in the locations of these slow anomalies among the models. A mean model computed only for the five tomographic models of the upper mantle shows no evidence for upper mantle upwellings (Fig. 7b).

Several of the tomographic models of the whole mantle show fast velocity anomalies in the upper mantle, which in many cases seem to be the anomaly associated with the cratonic lithosphere extended to greater depths (Figs. A.11 and A.13). In some models, we observe fast velocity anomalies at depths above and below the mantle transition zone (e.g., SG06, TX2007, SAW642ANb in Fig. A.13). These could perhaps be interpreted as fragments that detached from the lithosphere and sank into the sub-lithospheric mantle (Downey et al., 2011). However, the thirteen tomographic models of the whole mantle show little agreement concerning the presence of such anomalies (Figs. 7, A.10-A.13). Furthermore, taking into account that the tomographic resolution at mid-mantle depths is not very high, a scenario of lithospheric detachment is not supported by the available tomographic observations.

We conclude that observations from eighteen tomographic models (Figs. A.10-A.13) and their average, CMEAN2011 (Fig. 7), taken together with the large variability among the models, do not directly support a lithospheric anomaly below the Congo Basin, detached lithospheric fragments in the mantle, or asthenospheric uplift under the basin flanks. However, because the tomographic models for this region show such large differences compared to each other, it is possible that real structures are only imaged by a limited number of the models. A final evaluation would therefore require better convergence among the tomographic models under Central Africa.

5. Dynamic topography

Dynamic topography provides an additional, albeit indirect, constraint on the possible role of the sub-lithospheric mantle in the current isostatic state of the Congo Basin. We obtain an observation-based residual dynamic topography for the Congo Basin region (Fig. 8a) from the ETOPO1 topography by replacing sediments with crustal material that has a density of 2670 kg m^{-3}. In this calculation, we use a density difference between sediments and crust of 550 kg m^{-3} at the surface, linearly decreasing to 0 kg m^{-3} at 8 km depth. The observation-based residual dynamic topography is due to crustal thickness variations and density heterogeneities in the crust (beneath the sediments) and the mantle. It emphasizes a low in the Congo Basin area surrounded by dynamic topographic highs (Fig. 8a). The corresponding observation-based reduced Bouguer gravity anomaly of Fig. 8e uses the same sediment correction.

The dynamic topography predicted by our average tomographic model

CMEAN2011 (section 4 and Fig. 7) is shown in Fig. 8b and c. The tomography-derived dynamic topography is obtained by converting seismic wave speeds to density variations, assuming that both are caused by temperature variations. The conversion factor from relative S-wave speeds to relative density variations is depth-dependent with an average value of $\sim$0.25 (model M2b of Steinberger and Calderwood, 2006). Dynamic topography is computed with a viscous mantle flow model that only considers radial viscosity variations (Hager and O'Connell, 1979, 1981). We use viscosity model M2b of Steinberger and Calderwood (2006), which is tuned to match the observed global geoid, but modified for a 200 km thick viscous lithosphere. We use an incompressible mantle without phase changes and with a free-slip surface boundary condition, and calculate density differences with respect to the global density model PREM (Dziewonski and Anderson, 1981). Stresses acting on the lithosphere in this mantle flow model are converted to topography using a density contrast of 3300 kg m^{-3}, corresponding to the density of the uppermost mantle. We produce two different models where we disregard seismic velocity variations in the lithosphere above 150 km depth (in Fig. 8b) and 200 km depth (in Fig. 8c). These two models allow us to examine dynamic topography caused by density variations in the mantle and illustrate the role of the lowermost part of the craton in producing subsidence in the Congo Basin (Figs. 4 and 5). The cut-off depth of 200 km is based on the average lithospheric thickness for the Congo Craton (section 3), whereas the cut-off depth of 150 km is based on the recent suggestion that the lithosphere of the North American craton consists of a chemically depleted layer to approximately 150 km depth underlain by a thermal root which defines the lithosphere-asthenosphere boundary (Yuan and Romanowicz, 2010). Though no similar study exists for the Congo Craton, the model could perhaps also apply to other cratonic areas (King, 2005).

The tomography-derived dynamic topography shows a large low with a centre slightly offset from the centre of the Congo Basin (Fig. 8b, c). The dynamic topography predicted from CMEAN2011 is not too different in spatial extent or magnitude from the dynamic topographies predicted using S20RTS and TX2007 (Forte et al., 2010). The CMEAN2011 predicted dynamic topography low is larger, in absolute amplitude and spatial extent, than the observation-based residual dynamic topography, and encompasses even the high values of the latter. This probably reflects the effective resolution of the CMEAN2011 tomographic model. Figs. 8b and c illustrate that density anomalies in the lower part of the Congo Craton (150 - 200 km depth) could significantly contribute to dynamically-driven subsidence.

From the average tomographic model CMEAN2011 and the mantle flow model derived from it, a free-air gravity anomaly can be computed corresponding to the effects of internal density variations below 150 km depth (Fig. 8j) or 200 km depth (Fig. 8k) and the stresses at the surface and the core-mantle-boundary (Hager and O'Connell, 1979, 1981; Ricard et al., 1984; Richards and Hager, 1984; Steinberger and Calderwood, 2006). The free-air gravity calculated from CMEAN2011 has a low slightly to the north of the Congo Basin. When density anomalies in the deeper craton root are considered (Fig. 8j), this gravity low is slightly more negative than the low determined by sub-lithospheric density anomalies only (Fig. 8k). The Bouguer gravity anomaly calculated from CMEAN2011 (Fig. 8f and g) corresponds in shape and spatial extent to the predicted dynamic topography and also shows more negative gravity values when density anomalies in the lower part of the craton root are included.

The observation-based dynamic topography shows a low centred on the Congo Basin, indicating a potential role of density variations in the crust and mantle in the isostatic state of the Congo region. The dynamic topography computed from the average tomographic model CMEAN2011 predicts a low of similar magnitude from sub-lithospheric density anomalies, but over a larger area and with an offset relative to the observations (Fig. 8c). The tomography-derived dynamic topography illustrates that additional dynamic subsidence can be expected caused by density anomalies in the lower part of the Congo Craton (Figs. 8b, c).

6. Simple gravity models

The observed free-air and Bouguer gravity anomalies over the Congo Basin can be explained by the low-density sedimentary rocks in the basin (section 2, Kadima et al. (2011b), Crosby et al. (2010)). These low-density sediments need, however, an isostatic compensation for which several solutions have been put forward. Kadima et al. (2011b) suggest that compensation is at the depth of the Moho, in the form of crustal thinning inherited from the Neoproterozoic rifting phase. Downey and Gurnis (2009) show that a good fit to reduced present-day topography (reduced with the effect of Mesozoic - Cenozoic rocks) and free-air gravity can be obtained with a dynamic model in which a body about 1200 km wide and 100 - 200 km thick, with a density anomaly of 27 - 60 kg m^{-3}, is placed at 100 km depth within the lithosphere. On the other hand, Crosby et al. (2010) suggest that the Congo Craton, as cratons elsewhere, must have a chemically depleted root with a lower density. Therefore, Crosby et al. (2010) prefer a small convective asthenospheric drawdown below the basin. The tomography and gravity data that are available for the Congo region at present do not allow a definitive distinction between these scenarios.

For illustration purposes, we present a similar example to Downey and Gurnis (2009), but do not search for a best fit model to the gravity and topography data. Fig. 8d, h, and l shows dynamic topography, Bouguer gravity, and free-air gravity obtained from a Gaussian density anomaly, following $\Delta\rho_{max} \exp(-(r/r_0)^2)$ with $\Delta\rho_{max} = 1.8\%$, $r =$ distance in degrees to the centre of the anomaly at 1° S and 21° E, and $r_0 = 6°$. We place this anomaly at 100 - 200 km depth, which is within our lithospheric thickness of 200 km. Our example shows that the dynamic topography, reduced Bouguer, and free-air gravity data could be explained by a high density body within the cratonic lithosphere (Fig. 8d, h, and l). Note that the Congo Basin is a smaller scale feature in the middle of a regional large-scale positive dynamic topography (Fig. 8a). A discrepancy of 800 - 1000m exists in the colour scales for observation-based dynamic topography (Fig. 8a) and model-derived dynamic topography (Fig. 8d) because our model does not incorporate the regional, large-scale uplift, and has zero background topography. A corresponding offset (consistent with the Bouger correction) has been used for the Bouguer gravity colour scale (Fig. 8h).

The open question is how a dense anomaly within the cratonic root below the Congo Basin can be reconciled with global data that indicate chemical depletion, and hence a lower density, of cratonic roots (albeit with considerable scatter in the amount of depletion). We offer here the speculation, based on Yuan and Romanowicz (2010), that the upper part of the lithospheric root below the Congo Basin could be lighter because of chemical depletion, whereas its lower part could be thermally denser. As an example, we computed local Airy isostatic compensation and gravity anomalies for a vertical cylinder (Nettleton, 1942; Turcotte and Schubert, 2002) centred on the Congo Basin, relative to a continental reference column. One possible solution is shown in Fig. 9. It results in Airy isostatic equilibrium, a Bouguer gravity anomaly of -76 mGal, a reduced Bouguer anomaly of +2 mGal (reduced by the gravity signal of low density sedimentary rocks in the basin), and a free-air gravity anomaly of -39 mGal. We do note that various crustal and lithospheric structures could explain the Congo Basin gravity anomalies and that the data that are currently available for the Congo region do not allow studies to impose strong constraints on these speculative models.

7. Discussion

We have examined gravity data and seismic tomographic models to evaluate whether deposition of the Mesozoic - Cenozoic sedimentary rocks in the Congo Basin could have occurred in response to mantle processes. The available geological and geophysical data indicate that the Congo Basin probably initiated in a Neoproterozoic rift phase (Daly et al., 1992; Kadima et al., 2011b). The extension of the thick lithosphere underlying the basin could have led to a long post-rift subsidence phase, which would explain the slow tectonic subsidence over the Palaeozoic into the Mesozoic (Crosby et al., 2010; Kadima et al., 2011b). Several alternative explanations exist for the deposition of the uppermost ~1 km-thick, un-tilted, horizontal Mesozoic - Cenozoic rocks in the basin: (1) Subsidence occurred in response to viscous support of a dense body in the upper mantle (Downey and Gurnis, 2009). (2) The sediments were deposited in response to mantle upwellings below the basin flanks which caused a downward flow below the basin (Crosby et al., 2010). (3) Shallow mantle convection uplifted the basin flanks and shaped the Congo Basin as a sediment catchment area (Burke and Gunnell, 2008). (4) The post-rift phase extended into the Cenozoic. (5) Subsidence occurred following mantle downwelling associated with a detached lithosphere fragment.

Our analysis of lithospheric thickness and tomographic models of the upper mantle shows that the Congo Basin is underlain by a thick lithosphere. Based on lithospheric thickness values derived from tomographic models of the upper mantle, the Congo Craton could coincide with the outline of the present-day drainage basin (Fig. 5). This could point to a causal relation between the Congo Basin and its underlying craton, but a coincidental relation can not be ruled out. Crosby et al. (2010) have suggested that the most recent subsidence phase in the Congo Basin was produced by a convective downwelling in response to adjacent upwelling plumes at the basin edges. Asthenospheric flow fed from these plumes could have dragged cold material across the base of the lithosphere. This material could have converged and flowed down beneath the Congo Basin. Tectonic subsidence above downward mantle flow also occurs in the models of upper mantle-scale convection under a stationary plate of England and Houseman (1984). Their 2-D convection model creates dynamic subsidence over a length scale of nearly 1000 km, which is similar in order of magnitude to the Congo Basin. Nevertheless, the question remains if this length scale and flow pattern could vary significantly in 3-D mantle flow models, for different rheological models for the mantle and lithosphere, and for models with variable thicknesses of the continental lithosphere.

Our analysis of tomographic models of the upper and whole mantle demonstrates that there is little agreement among the seismic models concerning smaller-scale features that would indicate mantle upwellings (Figs. 7, A.10-A.13). This is mainly due to resolution issues and a lack of seismic coverage under the Congo Basin region. Most models show slow velocities (interpreted as warm upwellings) under the East African Rift, a large slow-velocity region in the lower mantle, and high velocities associated with the Congo Craton. The poor agreement over smaller-scale features makes it difficult to draw strong conclusions about the role of the mantle for the Congo Basin. We do note that we do not observe a consistent signal of fast velocity anomalies in the mantle below the Congo Craton. This means that most of the tomographic models do not support the hypothesis of lithospheric delamination (Downey et al., 2011) over relatively recent times (80 - 200 Ma for depths to 2000 km, assuming modest sinking rates).

Previous studies have pointed out that the negative gravity anomalies over the Congo Basin cannot be explained by density differences in the crust alone and that a dynamic mantle component is required (Hartley and Allen, 1994; Downey and Gurnis, 2009). Conversely, a correction for the negative gravity signal from the sediments in the basin reduces the free-air gravity anomaly considerably (Kadima et al., 2011b). In this study, we derive a residual Bouguer gravity field by applying a topographic correction to the EGM2008 free-air gravity (Pavlis et al., 2008) and by subtracting the negative gravity anomaly of the sediments in the Congo Basin (Fig. 2). Our analysis shows that the residual Bouguer gravity anomaly depends on the density values of the sedimentary rocks in the basin. We use different density models based on published values for the Congo Basin sedimentary units (Downey and Gurnis, 2009; Kadima et al., 2011b) and show that the residual Bouguer gravity anomaly can be slightly negative to slightly positive, depending on the sediment density model that is used (Fig. 2). Even though this can explain the gravity anomalies of the Congo Basin, it is unknown how these low-density sediments are isostatically compensated and whether this compensation introduces its own gravity anomalies. The solutions that have been put forward are (1) an uplift of the Moho inherited from the Neoproterozoic rifting phase (Kadima et al., 2011b), (2) a dense lithospheric body (Downey and Gurnis, 2009), or (3) a depleted lithospheric root with a small asthenospheric downwelling underneath the basin (Crosby et al., 2010). A variation in crustal thickness underneath the basin could provide a (partial) compensation mechanism, but dismisses any compensation by anomalies in the cratonic root under the Congo Basin. We speculate that it may be possible to reconcile the three proposed compensation hypotheses by considering a lithosphere which is depleted in its upper part down to about 150 km depth, thermally denser in its lower part (Yuan and Romanowicz, 2010), and with a small Moho uplift (Fig. 9). However, we stress that at present the available geophysical data do not allow to select among the proposed mechanisms for isostatic compensation of the Congo Basin.

Similarly, a more definitive conclusion regarding the mechanism that created the accommodation space for the deposition of the Mesozoic - Cenozoic sedimentary units would need better agreement among the tomography and gravity data than what is achieved at present. In light of the fact that observations from eighteen tomographic models and their average, CMEAN2011, do not directly support a role of the mantle in the more recent evolution phase of the Congo Basin, we would favour a simple scenario in which the Congo Basin initiated in Neoproterozoic rifting and the Mesozoic - Cenozoic sedimentary rocks were either deposited in the last stages of a very long post-rift phase or simply deposited on top of the basin floor. In the latter case, the deposition of the sediments would gradually have raised the basin floor to its present-day elevation of about 400 m above sea-level. Note that with a mantle density of 3250 kg m^{-3} and a sediment density of 2120 kg m^{-3}, 1 km of deposited sedimentary rocks would correspond to an uplift of about 350 m, which is similar to the present-day average elevation.

8. Conclusions

We have analysed gravity data and seismic tomographic models to evaluate whether the upper 1 km of Mesozoic - Cenozoic sedimentary rocks in the Congo Basin were deposited in response to mantle processes. We find that:

- The Congo Basin is associated with a negative Bouguer anomaly which is mainly produced by the negative gravity signal of the sedimentary units in the basin.

- The Congo Basin boundary could coincide with the boundary of the seismically-derived Congo Craton.

- The large variability between thirteen seismic tomographic models of the whole mantle does not support a deeper mantle source for producing the Mesozoic - Cenozoic subsidence in the Congo Basin.

- There are no convincing seismic velocity anomalies correlated to upward-directed mantle flow beneath the flanks of the Congo Basin in five tomographic models of the upper mantle.

- Anomalously high seismic velocities in the mantle beneath the Congo Basin at depths above ~300 km are a robust feature of mantle tomographic models and presumably highlight the Congo Craton.

- If these anomalies are associated with high densities, the joint signal of gravity anomalies and residual topography can be approximately explained (Downey and Gurnis, 2009)

Current seismic tomography and gravity data do not prove or disprove the various hypotheses put forward to explain the deposition of the Mesozoic - Cenozoic Congo Basin sedimentary rocks, but the large variability between the tomographic models indicates that it is unlikely that the mantle would play a major role in the subsidence of the Congo Basin. The Congo Basin probably initiated as a rift basin in the Neoproterozoic (Kadima et al., 2011b) and likely developed as a sediment catchment basin in the latest stages of its evolution (Burke and Gunnell, 2008). The deposition of the Mesozoic - Cenozoic rocks might not be caused by subsidence. Instead, the sediments could have raised the surface elevation to the present ∼400 m above sea-level, with subsidence merely being a consequence of the additional sediment load.

Acknowledgements

This project benefitted from funding through a Norwegian-German collaborative grant from the Norwegian Research Council and the Deutscher Akademischer Austausch Dienst. We thank all authors who so kindly made tomography data available to us: Michael Antolik, Thorsten Becker, Stewart Fishwick, Yu 'Jeff' Gu, Miaki Ishii, Sergei Lebedev, Michael Pasyanos, Keith Priestley, Catherine A. Rychert, and Nathan Simmons. We greatly appreciate their willingness to share their data! We thank Nathan Downey and Mike Gurnis for providing their sediment thickness data, Walter Mooney and Alexander Gubanov for their basement age data, Irina Artemieva for her 1°x1° TC1 model, and Joshua Kennerly (National Geospatial-Intelligence Agency) for the point survey data of Evrard et al. (1960). We appreciated the helpful reviews by Nicky White and Stewart Fishwick. Many of our figures were made using GMT (Wessel and Smith, 1991).

References

Al-Hajri, Y., White, N., Fishwick, S., 2009. Scales of transient convective support beneath Africa. Geology 37, 883-886, doi: 10.1130/G25703A.1

Amante, C. and B. W. Eakins, 2009. ETOPO1 1 Arc-Minute Global Relief Model: Procedures, Data Sources and Analysis. NOAA Technical Memorandum NESDIS NGDC-24, 19 pp.

Anka, Z., Séranne, J., di Primio, R., 2010. Evidence of a large upper-Cretaceous depocentre across the Continent-Ocean boundary of the Congo-Angola basin. Implications for palaeo-drainage and potential ultra-deep source rocks. Mar. Petr. Geol. 27(3), 601-611, doi:10.1016/j.marpetgeo.2009.08.015

Antolik, M., Gu, Yu.J., Ekström, G., Dziewonski, A.M., 2003. J362D28: a new joint model of compressional and shear velocity in the Earth's mantle. Geophys. J. Int. 153, 443-466

Artemieva, I.M., 2006. Global 1° x 1° thermal model TC1 for the continental lithosphere: Implications for lithosphere secular evolution. Tectonophysics 416, 245-277, doi:10.1016/j.tecto.2005.11.022

Ayele, A., 2002. Active compressional tectonics in central Africa and implications for plate tectonic models: evidence from fault mechanism studies of the 1998 earthquakes in the Congo Basin. J. Afr. Earth Sci. 35, 45-50

Armitage, J.J., Allen, P.A., 2010, Cratonic basins and the long-term subsidence history of continental interiors. J. Geol. Soc. Lond. 167, 61-70, doi:10.1144/0016-76492009-108

Bassin, C., Laske, G., Masters, G. 2000. The current limits of resolution for surface wave tomography in North America, Eos Trans. AGU, 81(48), Fall Meet. Suppl., Abstract S12A-03

Batumike, J.M., Griffin, W.L., O'Reilly, S.Y., 2009. Lithospheric mantle structure and the diamond potential of kimberlites in southern D.R. Congo. Lithos 112S, 166-176, doi: 10.1016/j.lithos.2009.04.020

Burke, K., Torsvik, T.H., 2004. Derivation of Large Igneous Provinces of the past 200 million years from long-term heterogeneities in the deep mantle. Earth Planet. Sci. Lett. 227, 531-538.

Burke, K., Gunnell, Y., 2008. The African Erosion Surface: A Continental-Scale Synthesis of Geomorphology, Tectonics, and Environmental Change over the Past 180 Million Years. Geol. Soc. Am. Mem. 201, 66 p., doi: 10.1130/2008.1201

Cahen, L., Ferrand, J.J., Haarsma, M.J.F., Lepersonne, J., Verbeek, Th., 1959. Description du sondage de Samba. Annales du Musée royal du Congo belge in-8°, Sc. géol. 29

Cahen, L., Ferrand, J.J., Haarsma, M.J.F., Lepersonne, J., Verbeek, Th., 1960. Description du sondage de Dekese. Annales du Musée royal du Congo belge in-8°, Sc. géol. 34

Craig, T.J., Jackson, J.A., Priestley, K., McKenzie, D., 2011. Earthquake distribution patterns in Africa: their relationship to variations in lithospheric and geological structure, and their rheological implications. Geophys. J. Int. 185, 403-434, doi: 10.1111/j.1365-246X.2011.04950.x

Conrad, C.P., Lithgow-Bertelloni, C., 2006. Influence of continental roots and asthenosphere on plate-mantle coupling. Geophys. Res. Lett. 33, L05312, doi:10.1029/2005GL025621

Crosby, A.G., Fishwick, S., White, N., 2010. Structure and evolution of the intracratonic Congo Basin. Geochem. Geophys. Geosys. 11(6), Q06010, doi:10.1029/2009GC003014

Delvaux, D., Barth, A., 2010. African stress pattern from formal inversion of focal mechanism data. Tectonophysics 482, 105-128

De Waele, B., Johnson, S.P., Pisarevsky, S.A., 2008. Palaeoproterozoic to Neoproterozoic growth and evolution of the eastern Congo Craton: Its role in the Rodinia puzzle. Precambrian Res., 160, 127-141.

Daly, M.C., Lawrence, S.R., Diemu-Tshiband, K., Matouana, B., 1992. Tectonic evolution of the Cuvette Centrale, Zaire. J. Geol. Soc. Lond. 149, 539-546, doi:10.1144/gsjgs.149.4.0539

Downey, N.J., Gurnis, M., 2009. Instantaneous dynamics of the cratonic Congo basin. J. Geophys. Res. 114, B06401, doi:10.1029/2008JB006066

Downey, N., Gurnis, M., Avouac, J.-P., 2011. Subsidence history and geodynamic evolution of the cratonic Congo Basin. Geophys. Res. Abstracts 13, EGU2011-388-1

Durek, J.J., Ekström, G., 1996. A radial model of anelasticity consistent with long-period surface-wave attenuation. Bull. Seism. Soc. Am. 86, 144-158,

Dziewonski, A.M., Anderson, D.L., 1981. Preliminary reference Earth model, Phys. Earth planet. Inter., 25, 297356

England, P., Houseman, G., 1984. On the geodynamic setting of kimberlite genesis. Earth Planet. Sci. Lett. 67, 109-122.

Evrard, P., Jones, L., Mathieu, Ph.L., 1960. Carte Gravimetrique. In: Jones, L., Mathieu, P.L., Strenger, H., Gravimetrie, Annales du Musée royal du Congo belge in-8°, Sc. géol. 36

Fishwick, S., 2010. Surface wave tomography: Imaging of the lithosphere - asthenosphere boundary beneath central and southern Africa? Lithos 120 (1-2), 63-73

Forte, A.M., Quéré, S., Moucha, R., Simmons, N.A., Grand, S.P., Mitrovica, J.X., Rowley, D.B., 2010. Joint seismic-geodynamic-mineral physical modelling of African geodynamics: A reconciliation of deep-mantle convection with surface geophysical constraints. Earth Planet. Sci. Lett. 295, 329-341, doi:10.1016/j.epsl.2010.03.017

Giresse, P., 2005. Mesozoic-Cenozoic history of the Congo Basin. J. Afr. Earth Sci. 43, 301-315

Grand, S.P., 2002. Mantle shear wave tomography and the fate of subducted slabs. Phil. Trans. R. Soc. Lond. A., 360, 2475-2492

Gu, Y.J., Dziewonski, A.M., Ekström, G., 2003. Simultaneous inversion for mantle shear velocity and topography of transition zone discontinuities. Geophys. J. Int. 154, 559-583

Gubanov, A.P., Mooney, W.D., 2009. New global geological maps of crustal basement age, Eos Trans. AGU 90(52), Fall Meet. Suppl, Abstract T53B-1583

Hager, B.H., O'Connell, R.J., 1979. Kinematic models of large-scale mantle flow. J. Geophys. Res., 84, 10311048

Hager, B.H., O'Connell, R.J., 1981. A simple global model of plate dynamics and mantle convection. J. Geophys. Res., 86, 48434867

Hartley, R.W., Allen, P.A., 1994. Interior cratonic basins of Africa: relation to continental break-up and role of mantle convection. Bas. Res. 6, 95-113

Jordan, T.H., 1978. Composition and development of the continental tectosphere. Nature 274, 544-548

Kadima, E., Delvaux, D., Sebagenzi, S.N., Tack, L., Kabeya, S.M., 2011a. Structure and geological history of the Congo Basin: an integrated interpretation of gravity, magnetic and reflection seismic data. Bas. Res. doi: 10.1111/j.1365-2117.2011.00500.x

Kadima, E. K., Ntabwoba, S.S.M., Lucazeau, F., 2011b. A Proterozoic-rift origin for the structure and the evolution of the Congo basin. Earth Planet. Sci. Lett. doi: 10.1016/j.epsl.2011.01.037

Kennett, B. L. N., and Engdahl, E.R., 1991. Traveltimes for global earthquake location and phase identification. Geophys. J. Int., 105, 429465

Kennett, B. L. N., Engdahl, E.R., Buland, R. 1995. Constraints on seismic velocities in the Earth from travel times. Geophys. J. Int., 122, 108124, doi:10.1111/j.1365- 246X.1995.tb03540.x

King, S.D., 2005. Archean cratons and mantle dynamics. Earth Planet. Sci. Lett., 234, 1-14, doi: 10.1016/j.epsl.2005.03.007

King, S.D., Ritsema, J., 2000. African hot spot volcanism: Small-scale convection in the upper mantle beneath cratons. Science, 290, 1137-1140.

Kustowski, B., Ekström, Dziewonski, A.M., 2008. Anisotropic shear-wave velocity structure of the Earths mantle: A global model. J. Geophys. Res. 113, B06306, doi:10.1029/2007JB005169

Laske, G., Masters, G., 1997. A global digital map of sediment thickness. EOS Trans. AGU, 78, F483.

Lawrence, S.R., Makazu, M.M., 1988. Zaire's central basin: prospectivity outlook. Oil & Gas Journal 86, 105-108.

Lebedev, S., van der Hilst, R.D., 2008. Global upper-mantle tomography with the automated multimode inversion of surface and S-wave forms. Geophys. J. Int., doi: 10.1111/j.1365-246X.2008.03721.x

Lekić, V., Panning, M., Romanowicz, B., 2010. A simple method for improving crustal corrections in waveform tomography. Geophys. J. Int., 182, 265-278, doi: 10.1111/j.1365-246X.2010.04602.x

Leturmy, P., Lucazeau, F., Brigaud, F., 2003. Dynamic interactions between the gulf of Guinea passive margin and the Congo River drainage basin: 1. Morphology and mass balance. J. Geophys. Res. 108, doi:10.1029/2002JB001927

Li, C., van der Hilst, R.D., Engdahl, E.R., Burdick, S., 2008. A new global model for P wave speed variations in Earth's mantle. Geochem. Geophys. Geosys. 9(5), Q05018, doi:10.1029/2007GC001806

Masters, G., Laske, G., Dahlen, F.A., Dziewonski, A.M., 2000. The Relative Behavior of Shear Velocity, Bulk Sound Speed, and Compressional Velocity in the Mantle: Implications for Chemical and Thermal Structure. In:

Earth's Deep Interior, Karato, S., Forte, A.M., Liebermann, R.C., Masters, G., Stixrude, L. (eds), AGU Monograph 117

Meert, J.G., 2003. A synopsis of events related to the assembly of eastern Gondwana. Tectonophysics 362, 1-40.

Mégnin, C., Romanowicz, B., 2000. The three-dimensional shear velocity structure of the mantle from the inversion of body, surface and higher-mode waveforms. Geophys. J. Int., 143, 709-728

Montelli, R., Nolet, G., Dahlen, F.A., Masters, G., 2006. A catalogue of deep mantle plumes: New results from finite frequency tomography. Geochem. Geophys. Geosys. 7(11), Q11007, doi: 10.1029/2006GC001248

Mooney, W.D., Laske, G., Masters, G. 1998. CRUST-5.1: a global crustal model at 5° x 5°. J. Geophys. Res., 103, 727747

Nataf, H.C.,Ricard, Y. 1996. 3SMAC: an a priori tomographic model of the upper mantle based on geophysical modeling. Phys. Earth. Planet. Int., 95, 10122

Nettleton, L.L., 1942. Gravity and magnetic calculations. Geophysics, 7, 293-310

Nyblade, A.A., Robison, S.W., 1994. The African Superswell. Geophys. Res. Lett., 21, 765-768.

Panning, M.P., Lekić, V., Romanowicz, B.A., 2010. Importance of crustal corrections in the development of a new global model of radial anisotropy. J. Geophys. Res., 115, B12325, doi:10.1029/2010JB007520

Pasyanos, M.E., Nyblade, A.A., 2007. A top to bottom lithospheric study of Africa and Arabia. Tectonophysics 444, 27-44, doi:10.1016/j.tecto.2007.07.008

Pavlis, N.K., Holmes, S.A., Kenyon, S.C. and Factor, J.K., 2008. An Earth Gravitational Model to degree 2160, EGU2008-A-01891, http://earth-info.nga.mil/GandG/wgs84/gravitymod/egm2008/index.html

Priestley, K., McKenzie, D., Debayle, E., Pilidou, S., 2008. The African upper mantle and its relationship to tectonics and surface geology. Geophys. J. Int., 175, 1108-1126, doi: 10.1111/j.1365-246X.2008.03951.x

Ricard, Y., Fleitout, L., Froidevaux, C., 1984. Geoid heights and lithospheric stresses for a dynamic Earth. Ann. Geophys., 2, 267286

Richards, M.A., Hager, B.H., 1984. Geoid anomalies in a dynamic Earth. J. Geophys. Res., 89, 59876002

Ritsema, J., van Heijst, H.J., Woodhouse, J.H., 2004. Global transition zone tomography. J. Geophys. Res. 109, B02302, doi:10.1029/2003JB002610

Ritsema, J., Deuss, A., van Heijst, H.J., Woodhouse, J.H., 2011. S40RTS: a degree-40 shear-velocity model for the mantle from new Rayleigh wave dispersion, teleseismic traveltime and normal-mode splitting function measurements. Geophys. J. Int., 184, 1223-1236, doi: 10.1111/j.1365-246X.2010.04884.x

Sahagian, D.L., 1993. Structural evolution of African basins: stratigraphic synthesis. Bas. Res. 5, 41-54

Shapiro, N.M., Ritzwoller, M.H., 2002. Monte-Carlo inversion for a global shear-velocity model of the crust and upper mantle. Geophys. J. Int. 151, 88-105

Simmons, N.A., Forte, A.M., Grand, S.P., 2007. Thermochemical structure and dynamics of the African superplume. Geophys. Res. Lett. 34, L02301. doi:10.1029/2006GL028009

Steinberger, B., Torsvik, T.H., 2008. Absolute plate motions and true polar wander in the absence of hotspot tracks. Nature 452, 620-623, doi:10.1038/nature06824

Steinberger, B., Calderwood, A., 2006. Models of large-scale viscous flow in the Earth's mantle with constraints from mineral physics and surface observations. Geophys. J. Int. 167, 1461-1481.

Steinberger, B., Holme, R., 2008. Mantle flow models with core-mantle boundary constraints and chemical heterogeneities in the lowermost mantle. J. Geophys. Res. 113, B05403, doi: 10.1029/2007JB005080

Torsvik, T.H., Müller, R.D., Van der Voo, R., Steinberger, B., Gaina, G., 2008. Global plate motion frames: Towards a unified model. Rev. Geophys. 46, RG3004, doi:10.1029/2007RG000227

Torsvik, T.H., Rousse, S., Labails, C., Smethurst, M.A., 2009. A new scheme for the opening of the South Atlantic Ocean and the dissection of an Aptian salt basin. Geophys. J. Int., 177, 1315-1333

Toteu, S.F., van Schmus, W.R., Penaye, J., Nyobé, 1994. U-Pb and Sm-Nd evidence for Eburnian and Pan-African high-grade metamorphism in cratonic rocks of southern Cameroon. Precambrian Res. 67, 321-347.

Turcotte, D.L., Schubert, G., 2002. Geodynamics, second edition. Cambridge University Press, 456 pp.

Van der Meer, D.G., Spakman, W., van Hinsbergen, D.J.J., Amaru, M.L., Torsvik, T.H., 2009. Towards absolute plate motions constrained by lower-mantle slab remnants. Nature Geoscience, 3, DOI: 10.1038/NGEO708

Wessel, P., Smith, W.H.F., 1991. Free software helps map and display data. EOS Trans. AGU, 72, 441

Xie, X., Heller, P.L., 2009. Plate tectonics and basin subsidence history. GSA Bulletin, 121, 55-64, doi: 10.1130/B26398.1

Yuan, H., Romanowicz, B., 2010. Lithospheric layering in the North American craton. Nature 466, 1063-1068, doi: 10.1038/nature09332

Name	Wave Type	Ref Model	Crust Model	Horz Res[a] (km)	Vert Res	Max Depth (km)	Stand Dev[b] (%)	Ref
Whole mantle								
MITP08	P	ak135[c]	CRUST2.0[d]	80	64 layers	CMB	0.247	Li et al. (2008)
P362D28	P	PREM[e]	CRUST5.1[f]	1100	14 splines	CMB	0.445	Antolik et al. (2003)
PRI-P05	P	iasp91[g]	CRUST2.0	300 - 800	not reported	CMB	0.387	Montelli et al. (2006)
PRI-S05	S	iasp91	CRUST2.0	300 - 800	not reported	CMB	0.806	Montelli et al. (2006)
S40RTS	S	PREM	CRUST2.0	500	21 splines	CMB	0.852	Ritsema et al. (2011)
S362ANI	S	STW105	CRUST5.1	1100	14 splines	CMB	1.594	Kustowski et al. (2008)
S362D28	S	PREM	CRUST5.1	1100	14 splines	CMB	1.593	Antolik et al. (2003)
SAW24B16	S	PREM	Inv[h]	830	16 splines	CMB	1.050	Mégnin and Romanowicz (2000)
SAW642ANb	S	PREM, QL6[i]	Inv[h,j]	830	16 splines	CMB	1.031	Panning et al. (2010)
SB4L18	S	PREM	CRUST5.1	1000	18 splines	CMB	1.201	Masters et al. (2000)
SG06	S	TNA/SNA, PREM	CRUST5.1	275	22 layers	CMB	1.305	Grand (2002)[k]
TOPOS362D1	S	PREM	CRUST5.1	1100	14 splines	CMB	1.458	Gu et al. (2003)
TX2007	S	TNA/SNA, PREM	CRUST5.1	250	22 layers	CMB	1.408	Simmons et al. (2007)
Upper mantle								
CU_SRT1.0	S	ak135	CRUST5.1	200	73 layers	250	2.018	Shapiro and Ritzwoller (2002)
CU_SDT1.0	S	ak135	CRUST5.1	200	73 layers	250	2.300	Shapiro and Ritzwoller (2002)
KP08	S	mod PREM	3SMAC[l]	400	16 layers	400	1.603	Priestley et al. (2008)
LH08	S	ak135	CRUST2.0	400	16 layers	661	1.854	Lebedev and Van der Hilst (2008)
SF09	S	ak135	3SMAC	400	16 layers	350	2.908	Fishwick (2010)

Table 1: List of tomography models. [a] Cell-size or half-wavelength, [b] Standard deviation of velocity anomalies over the larger Congo region (15°N-23°S, 5°E-36°E) and depth range of the tomography model, [c] Kennett et al. (1995), [d] Bassin et al. (2000), [e] Dziewonski and Anderson (1981), [f] Mooney et al. (1998), [g] Kennett and Engdahl (1991), [h] Crustal contributions and event source parameters are determined within the inversion, [i] Durek and Ekström (1996), [j] Lekić et al. (2010), [k] Model version of 2006, [l] Nataf and Ricard (1996).

Figure 1: a) Topography of the Congo Basin (ETOPO1 Amante and Eakins, 2009), with the location of the four deep wells (S = Samba, D = Dekese, G = Gilson-1, M = Mbandaka-1). b) Free-air gravity anomaly (EGM2008, Pavlis et al., 2008). c) Bouguer gravity anomaly computed from EGM2008 using a 2670 kg m^{-3} density correction. d) Free-air gravity anomaly from Evrard et al. (1960).

Figure 2: a) Mesozoic-Cenozoic sediment thickness from Downey and Gurnis (2009). b) and c) Total sediment thickness smoothed by spherical expansion to degree 511 from Laske and Masters (1997). d) Bouguer gravity signal from the Mesozoic-Cenozoic sediments in a), using a density difference between sediments and crust of 550 kg m^{-3}. e) Bouguer gravity signal from total sediment thickness in b) using a density difference between sediments and crust of 420 kg m^{-3} at the surface, decreasing to 0 kg m^{-3} at 8 km depth. f) Bouguer gravity signal from total sediment thickness in b) using a density difference between sediments and crust of 670 kg m^{-3} at the surface, decreasing to 0 kg m^{-3} at 8 km depth. g) Bouguer gravity field reduced with the gravity signal of the Mesozoic-Cenozoic sediments (panel d). h) Bouguer gravity field reduced with the gravity signal of the total sediments using a density difference of 420 to 0 kg m^{-3} (panel e). i) Bouguer gravity field reduced with the gravity signal of the total sediments using a density difference of 670 to 0 kg m^{-3} (panel f).

Figure 3: a) Age of crustal basement in the Congo region from Gubanov and Mooney (2009). The ages reflect either the time of crustal formation or the time of thermal or tectonic crustal reworking. The Congo Craton could tentatively be outlined by the area with ages > 1 Ga. b) Simplified geology map after De Waele et al. (2008) showing Archean kernels and Proterozoic-Cambrian belts. LV = Lake Victoria.

Figure 4: Lithosphere thickness models from: a) Artemieva (2006) (TC1 model). b) Conrad and Lithgow-Bertelloni (2006). c) Fishwick (2010). d) Pasyanos and Nyblade (2007). e) Priestley et al. (2008). The white areas in a)-c) represent areas in which data are either absent or unreliable (as determined by the authors of the models). f) Mean model of the five models in a) to e). The mean model has sharp transitions to the northeast and southwest of the Congo Basin due to domains without thickness data in the model of Conrad and Lithgow-Bertelloni (2006) (white regions in b)). g) Standard deviation (in km) of the models in a) to e). h) Topography (Fig. 1a) with superimposed the 200 km thick lithosphere outline of the mean model (from panel f). All models, except panels g and h, are plotted with the thickness scale shown in the bottomleft of the figure (below panel e).

Figure 5: Lithosphere thickness from upper mantle tomography models: a) CU_SRT1.0 (Shapiro and Ritzwoller, 2002), b) CU_SDT1.0 (Shapiro and Ritzwoller, 2002), c) KP08 (Priestley et al., 2008), d) LH08 (Lebedev and Van der Hilst, 2008), and e) SF09 (Fishwick, 2010). The lithosphere thickness is derived from the upper mantle tomography models by equating the depth down to which the velocity anomaly is consistently above +2% to lithosphere depth (following Conrad and Lithgow-Bertelloni, 2006). Lithosphere thickness smaller than 100 km is left blank in a)-e). f) Shows percentage of the domain in which the five models have a lithosphere thickness > 200 km. 100% means that all five models have thickness > 200 km, 20% means that only one model has thickness > 200 km. g) Topography (Fig. 1a) with superimposed the 200 km lithosphere thickness outline based on the 80% contour of panel f).

Figure 6: Motion of Africa relative to the mantle over the last 320 Ma. The line connecting filled circles shows the motion of a point at the centre of the Congo Basin. Africa's motion is calculated using a moving hotspot reference frame between 0-100 Ma and a palaeomagnetic reference frame before that, with a shift in longitude to achieve a smooth transition at 100 Ma (Torsvik et al., 2008). In addition, the palaeomagnetic reference frame is corrected for true polar wander (Steinberger and Torsvik, 2008).

Figure 7: Visualisation of the mean tomography model CMEAN2011. The mean model is an average of 10 S-wave and 3 P-wave whole mantle models below 250 km, and of 10 whole- and 5 upper-mantle S-wave models above 250 km depth (Table 1). Standard deviation (std dev) is computed from the spread between individual models. a) Map view at 200 km depth. b) Map view at 200 km depth from averaging the 5 upper-mantle S-wave models only (UM = upper mantle). c) Map view at 500 km depth. d) Map view at 800 km depth. e) SW-NE cross-section 1, f) NW-SE cross-section 2, and g) 3D view from the north, contouring the 0.5% velocity anomaly isosurfaces.

Figure 8: Dynamic topography (top), Bouguer gravity (middle), and free-air gravity (bottom). a) Observation-based dynamic topography. The residual dynamic topography is the ETOPO1 topography (Amante and Eakins, 2009) corrected isostatically for the sediments in the basin, by replacing the sediments with crustal material (using a density difference of 550 kg m^{-3} at the surface linearly decreasing to 0 kg m^{-3} at 8 km depth). b) Modelled dynamic topography based on the mean tomography model CMEAN2011 (Fig. 7), disregarding density anomalies above 150 km depth. c) As b), but with a cut-off depth of 200 km for density anomalies. d) Synthetic modelled dynamic topography based on a Gaussian density anomaly between 1° S and 21° E, and 100 and 200 km depth. The colour scale is shifted relative to a) by 1000 m. This corresponds to assuming that the dynamic topography low is superposed onto a larger-scale topography high. e) Observation-based Bouguer gravity anomalies from EGM2008 (Pavlis et al., 2008), smoothed by spherical expansion to degree 63 (which is the maximum degree to which the our CMEAN2011 model is expanded), and reduced with the gravity anomaly from the sedimentary rocks in the Congo Basin (using the same correction as in a). f) Modelled Bouguer gravity anomalies based on the mean tomography model CMEAN2011 (Fig. 7) with a cut-off depth of 150 km. g) As f), but with a cut-off depth of 200 km. h) Synthetic modelled Bouguer gravity anomaly based on the Gaussian density anomaly of d). i) Observation-based free-air gravity anomalies from EGM2008 (Pavlis et al., 2008), smoothed by spherical expansion to degree 63. j) Modelled free-air gravity anomalies based on the mean tomography model CMEAN2011 (Fig. 7) with a cut-off depth of 150 km. k) As j), but with a cut-off depth of 200 km. l) Synthetic modelled free-air gravity anomaly based on the Gaussian density anomaly of d).

Figure 9: Simple example of a Congo lithosphere structure that is in local isostatic equilibrium with a continental reference column. This example has an average reference crustal density of 2850 kgm^{-3}, a depleted upper lithosphere under Congo underlain by a dense lower lithosphere. The Bouguer gravity anomaly for the Congo column is -76 mGal, the reduced Bouguer gravity is +2 mGal (reduced by the gravity signal from the sedimentary units in the basin), and the free-air anomaly is -39 mGal. In the gravity calculation for a vertical cylinder (Nettleton, 1942; Turcotte and Schubert, 2002), the contribution of bodies with an anomalous density decreases with depth. Therefore a column in Airy isosatic equilibrium can have a non-zero free-air gravity anomaly.

Appendix A. Map views and cross-sections for 18 tomography models

Figure A.10: Map views at 200 km depth through 13 whole-mantle tomography models, 5 upper mantle models (Table 1) and the mean model CMEAN2011.

Figure A.11: Map views at 500 km depth through 13 whole-mantle tomography models, 1 upper mantle model (Table 1) and the mean model CMEAN2011.

Figure A.12: Map views at 800 km depth through 13 whole-mantle tomography models (Table 1) and the mean model CMEAN2011.

Figure A.13: Cross-sections through 13 whole-mantle tomography models (Table 1) and the mean model CMEAN2011. A) SW-NE cross-section 1, B) NW-SE cross-section 2. See Figs. 7, and A.10-A.12 for location of the cross-sections.

Figure 1

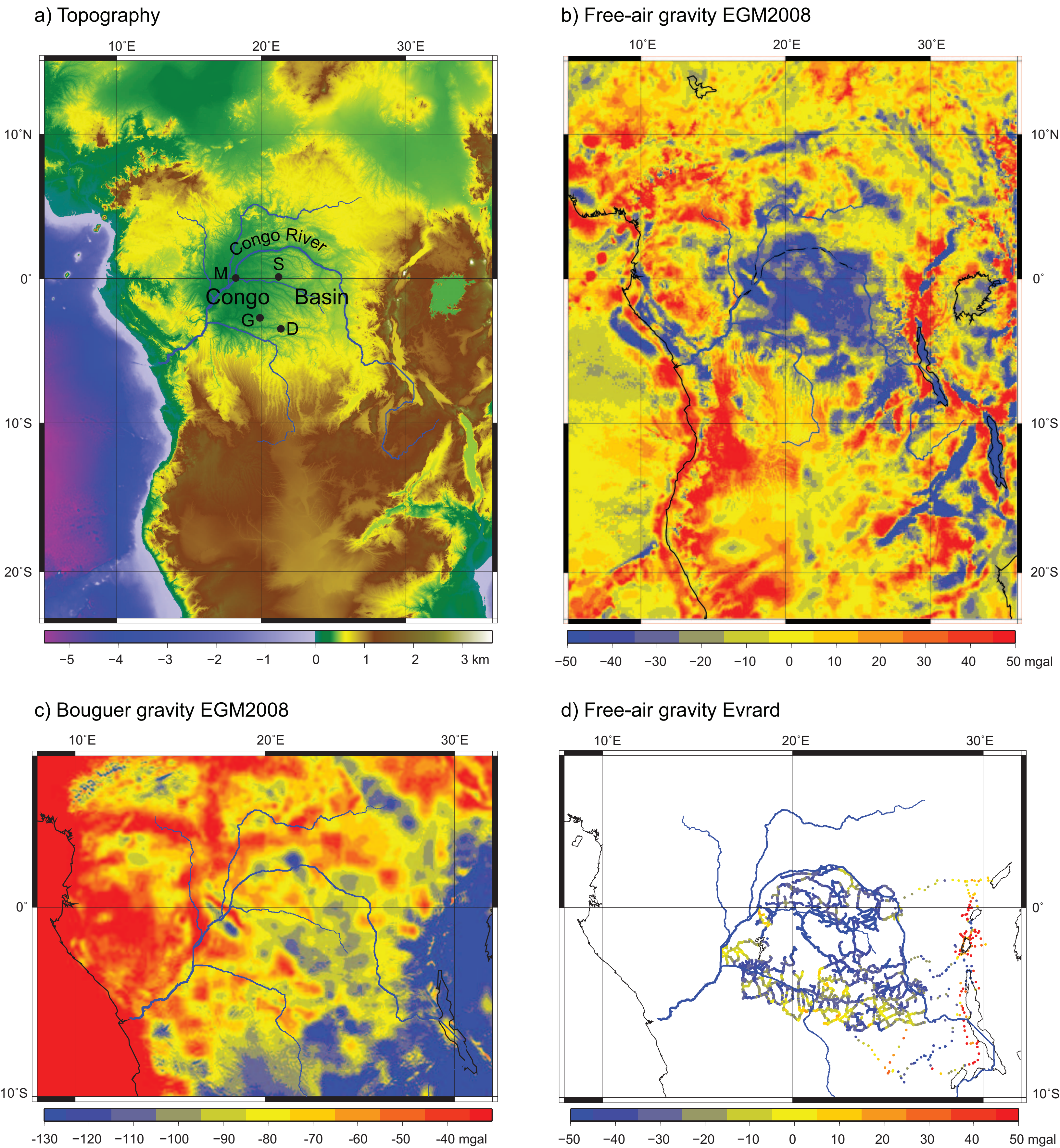

a) Topography
10˚E
20˚E
30˚E
10˚N
0˚
10˚S
20˚S
Congo River
M
S
Congo
Basin
G
D
−5
−4
−3
−2
−1
0
1
2
3 km
b) Free-air gravity EGM2008
−50
−40
−30
−20
−10
0
10
20
30
40
50 mgal
c) Bouguer gravity EGM2008
-130
−120
−110
−100
−90
-80
-70
-60
-50
-40 mgal
d) Free-air gravity Evrard

Figure 2

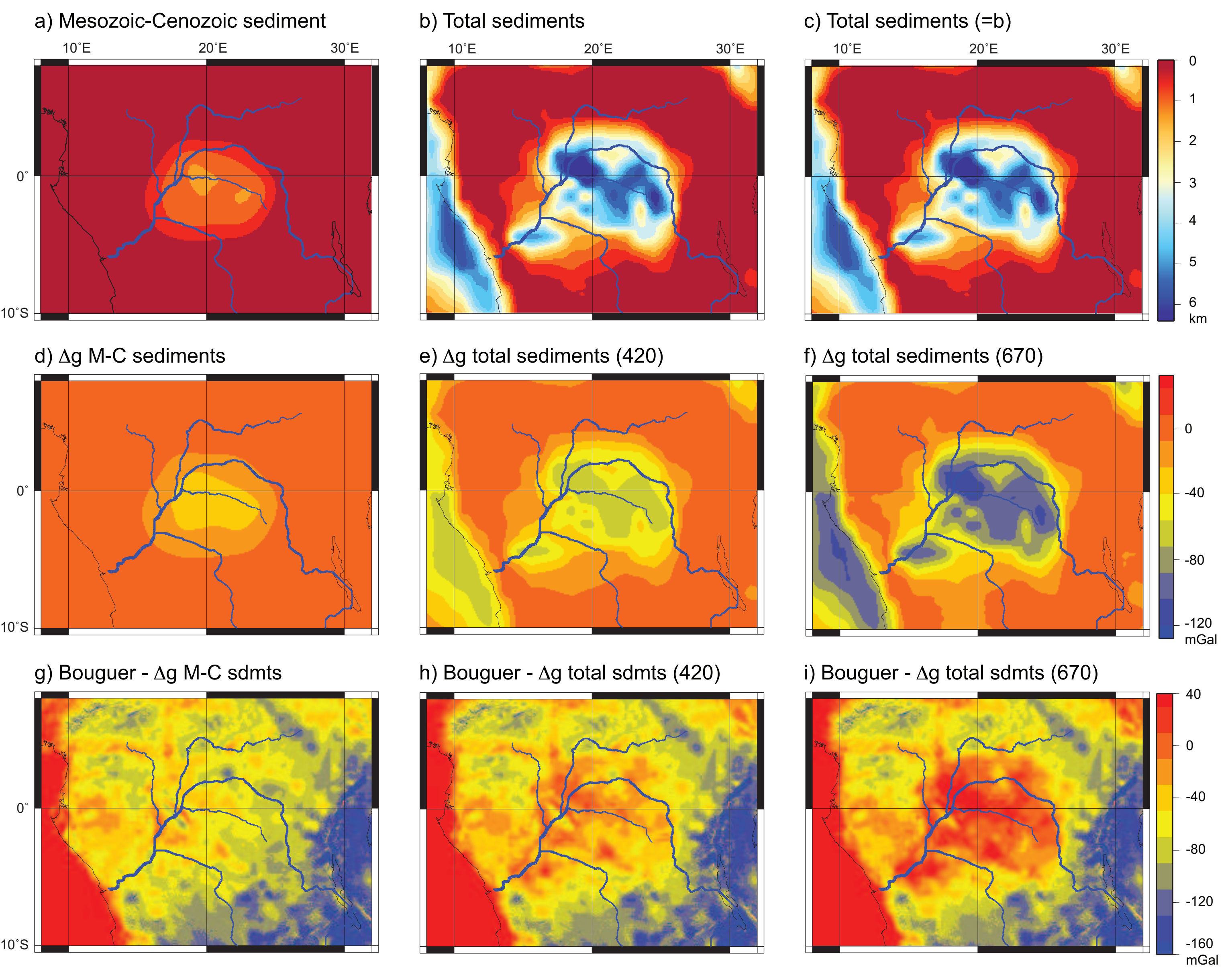
a) Mesozoic-Cenozoic sediment
b) Total sediments
c) Total sediments (=b)
10˚E
20˚E
30˚E
0˚
10˚S
0
1
2
3
4
5
6
km
d) Δg M-C sediments
e) Δg total sediments (420)
f) Δg total sediments (670)
0
-40
-80
-120
mGal
g) Bouguer - Δg M-C sdmts
h) Bouguer - Δg total sdmts (420)
i) Bouguer - Δg total sdmts (670)
40
0
-40
-80
-120
-160
mGal

Figure 3

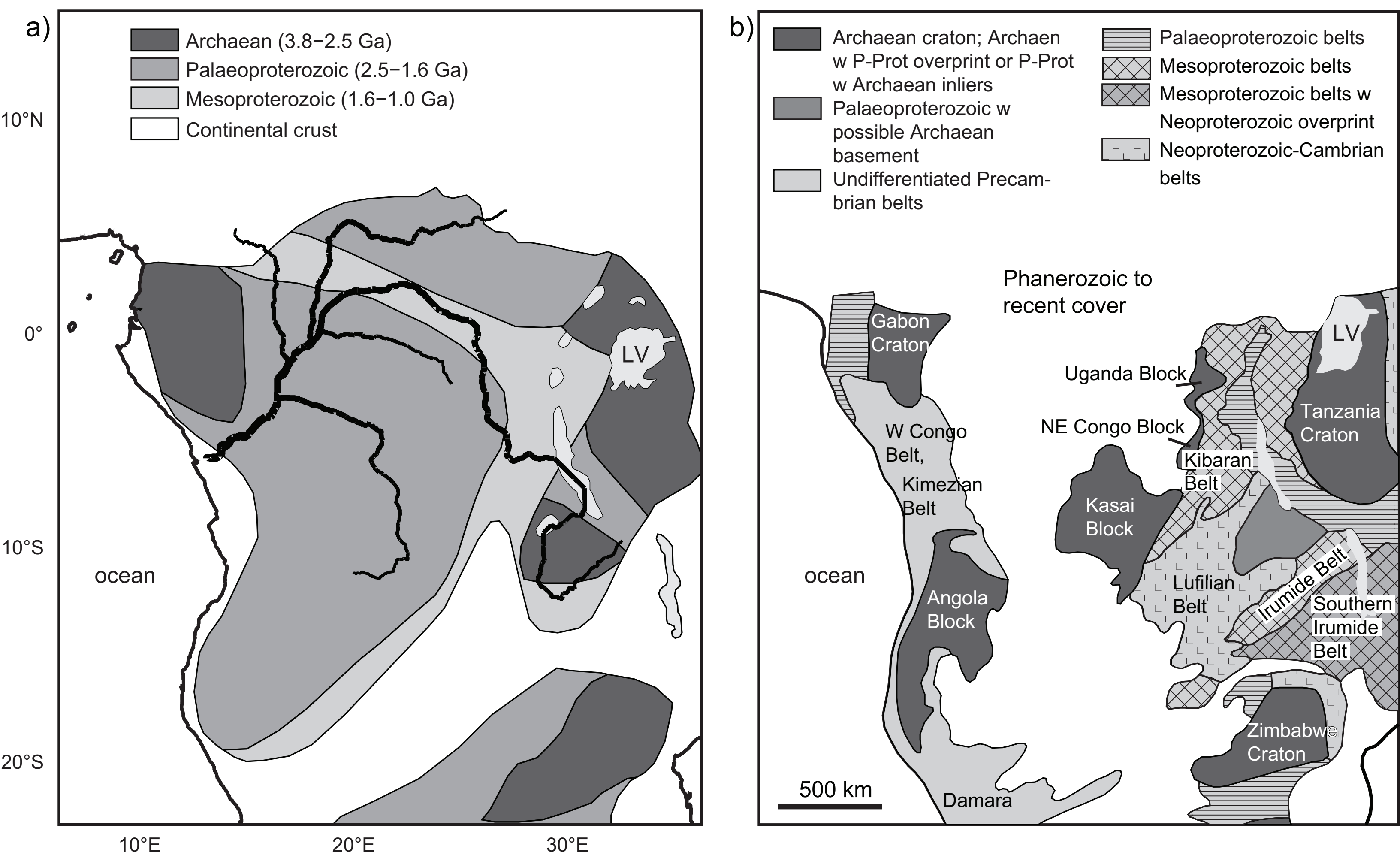
a)
Archaean (3.8−2.5 Ga)
Palaeoproterozoic (2.5−1.6 Ga)
Mesoproterozoic (1.6−1.0 Ga)
Continental crust
10°N
0°
10°S
20°S
10°E
20°E
30°E
ocean
LV
b)
Archaean craton; Archaen w P-Prot overprint or P-Prot w Archaean inliers
Palaeoproterozoic w possible Archaean basement
Undifferentiated Precambrian belts
Palaeoproterozoic belts
Mesoproterozoic belts
Mesoproterozoic belts w Neoproterozoic overprint
Neoproterozoic-Cambrian belts
Phanerozoic to recent cover
Gabon Craton
W Congo Belt, Kimezian Belt
Angola Block
Damara
Kasai Block
Uganda Block
NE Congo Block
Kibaran Belt
Lufilian Belt
Irumide Belt
Southern Irumide Belt
Tanzania Craton
LV
Zimbabwe Craton
ocean
500 km

Figure 4

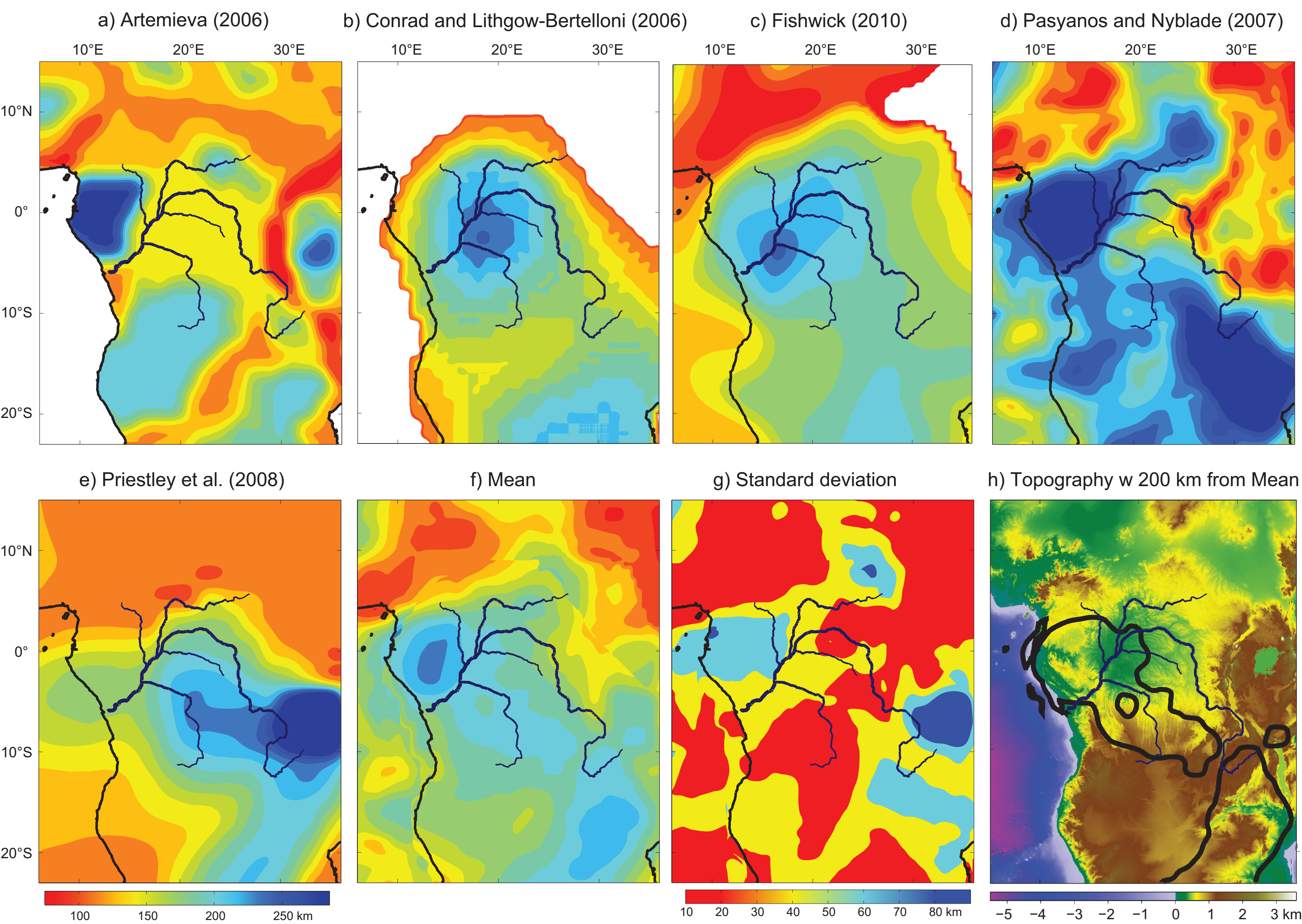
a) Artemieva (2006)
b) Conrad and Lithgow-Bertelloni (2006)
c) Fishwick (2010)
d) Pasyanos and Nyblade (2007)
10°E
20°E
30°E
10°N
0°
10°S
20°S
e) Priestley et al. (2008)
f) Mean
g) Standard deviation
h) Topography w 200 km from Mean
100
150
200
250 km
10
20
30
40
50
60
70
80 km
−5
−4
−3
−2
−1
0
1
2
3 km

Figure 5

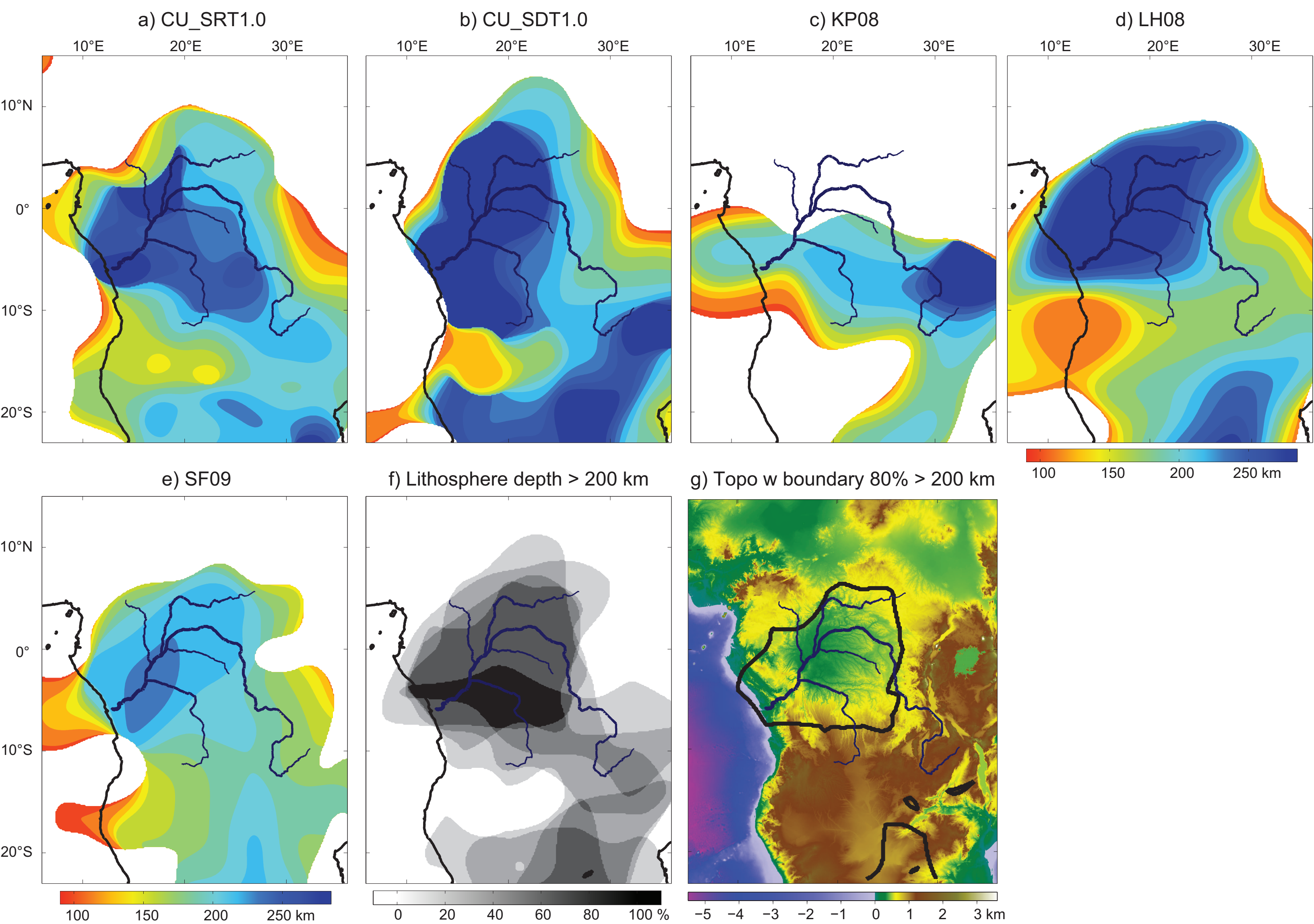

a) CU_SRT1.0
b) CU_SDT1.0
c) KP08
d) LH08
e) SF09
f) Lithosphere depth > 200 km
g) Topo w boundary 80% > 200 km
10°E
20°E
30°E
10°N
0°
10°S
20°S
100
150
200
250 km
0
20
40
60
80
100 %
−5
−4
−3
−2
−1
0
1
2
3 km

Figure 6

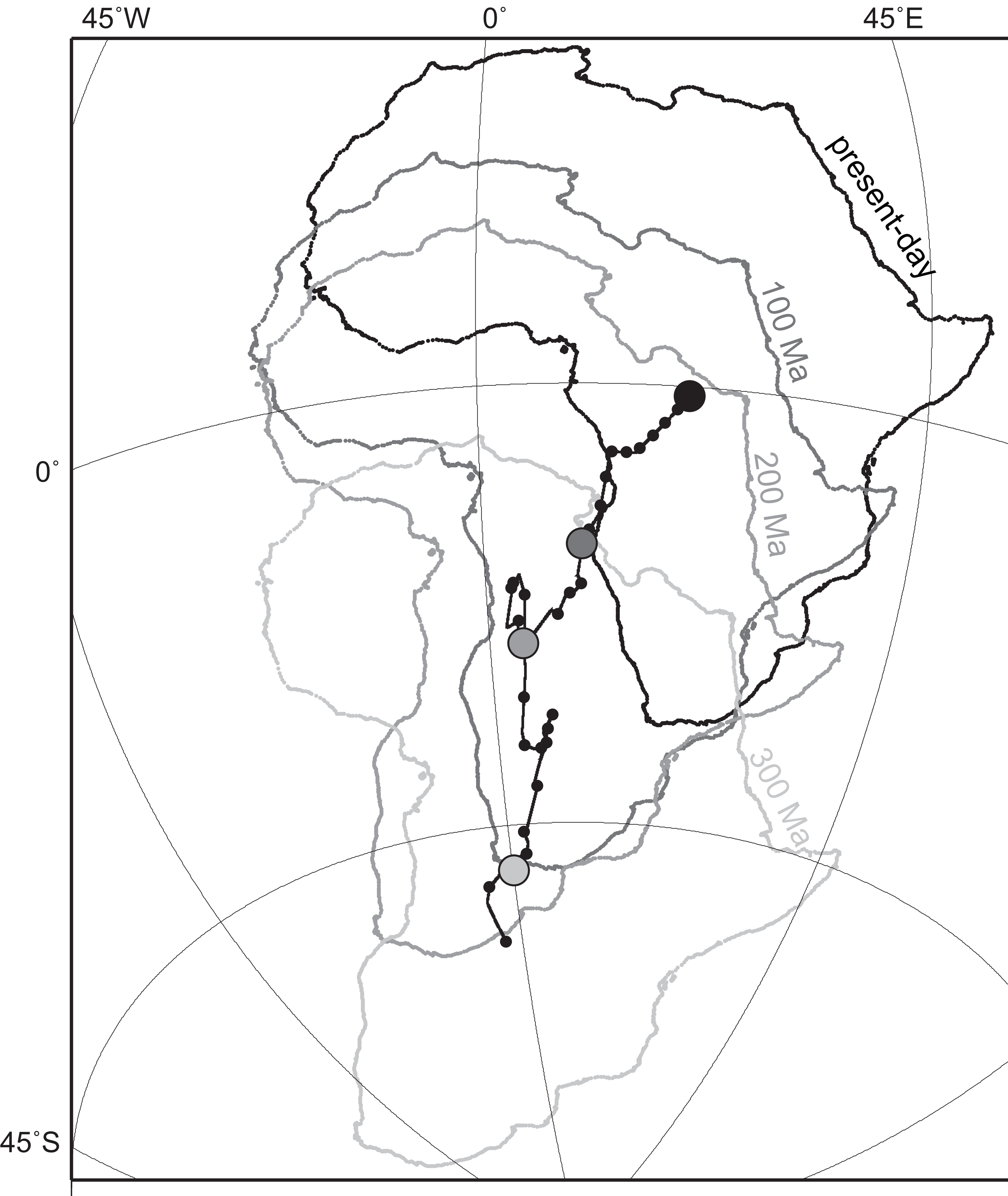

Figure 7

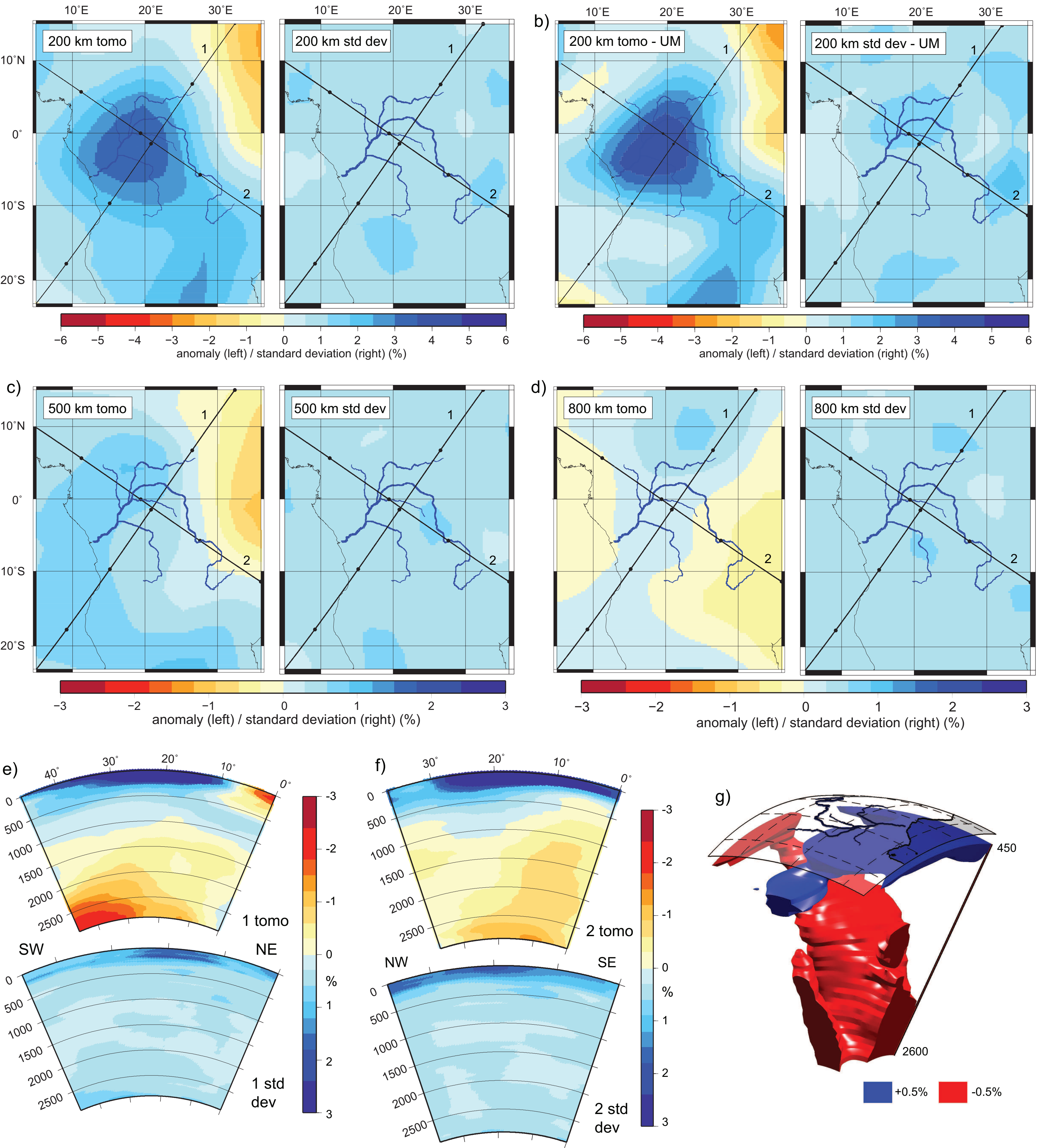

b)
c)
d)
e)
f)
g)
200 km tomo
200 km std dev
200 km tomo - UM
200 km std dev - UM
500 km tomo
500 km std dev
800 km tomo
800 km std dev
10°E
20°E
30°E
10°N
0°
10°S
20°S
anomaly (left) / standard deviation (right) (%)
1 tomo
1 std dev
2 tomo
2 std dev
SW
NE
NW
SE
%
450
2600
+0.5%
-0.5%

Figure 8

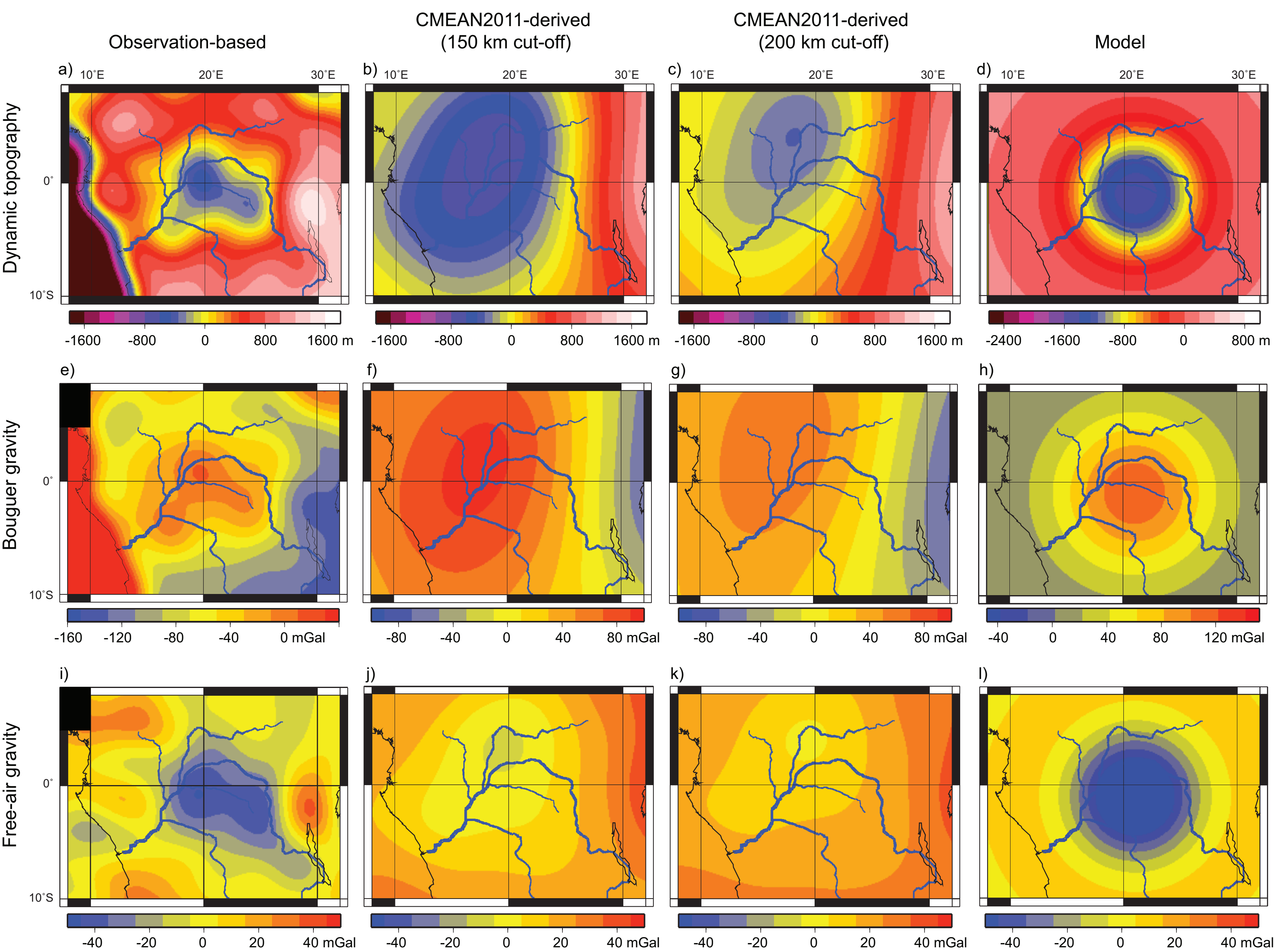

Observation-based
CMEAN2011-derived
(150 km cut-off)
CMEAN2011-derived
(200 km cut-off)
Model
Dynamic topography
Bouguer gravity
Free-air gravity
a)
b)
c)
d)
e)
f)
g)
h)
i)
j)
k)
l)
10˚E
20˚E
30˚E
0˚
10˚S
-1600
-800
0
800
1600 m
-2400
-1600
-800
0
800 m
-160
-120
-80
-40
0 mGal
-80
-40
0
40
80 mGal
-40
0
40
80
120 mGal
-40
-20
0
20
40 mGal

Figure 9

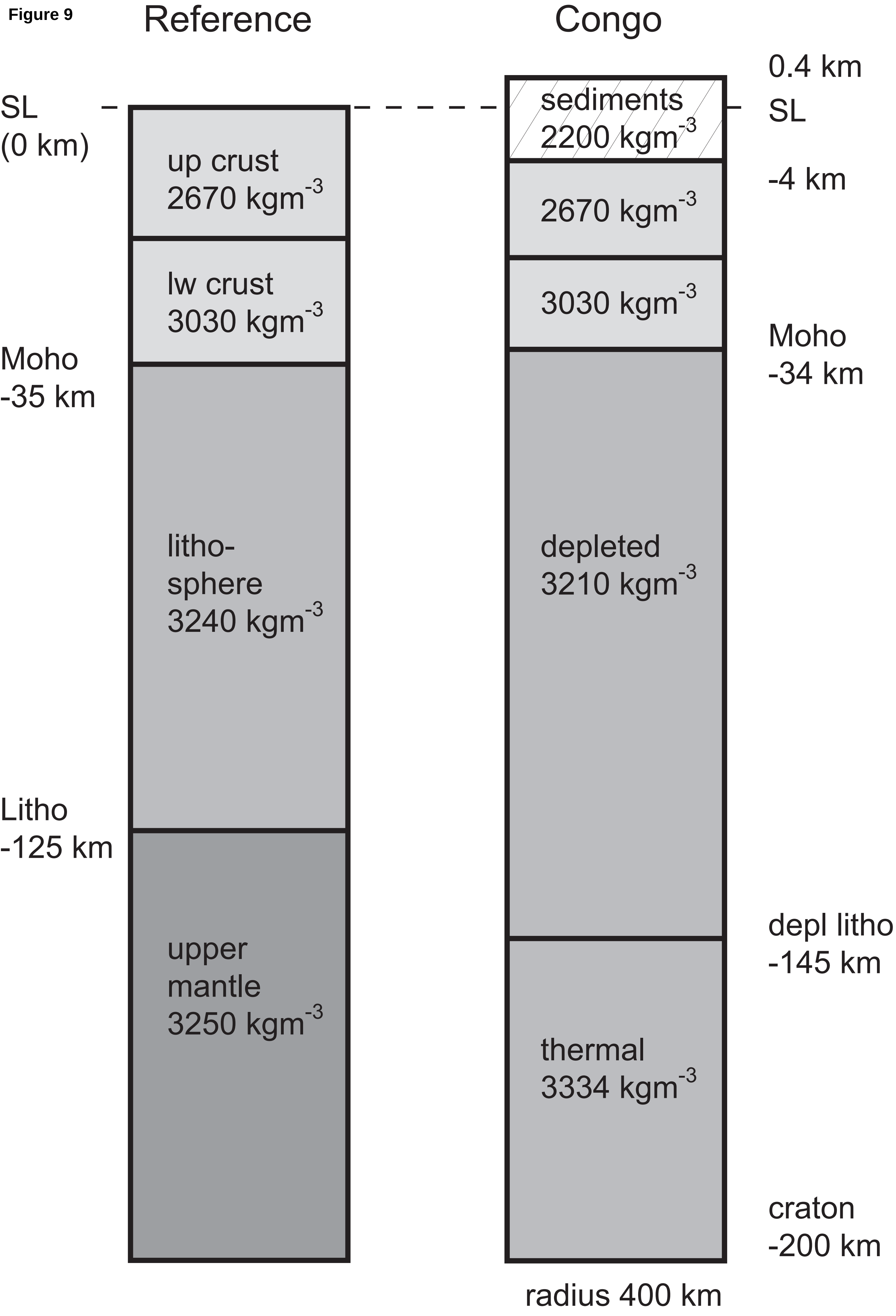
Reference
Congo
SL
(0 km)
up crust
2670 kgm-3
lw crust
3030 kgm-3
Moho
-35 km
litho-
sphere
3240 kgm-3
Litho
-125 km
upper
mantle
3250 kgm-3
0.4 km
SL
sediments
2200 kgm-3
-4 km
2670 kgm-3
3030 kgm-3
Moho
-34 km
depleted
3210 kgm-3
depl litho
-145 km
thermal
3334 kgm-3
craton
-200 km
radius 400 km

Figure 10

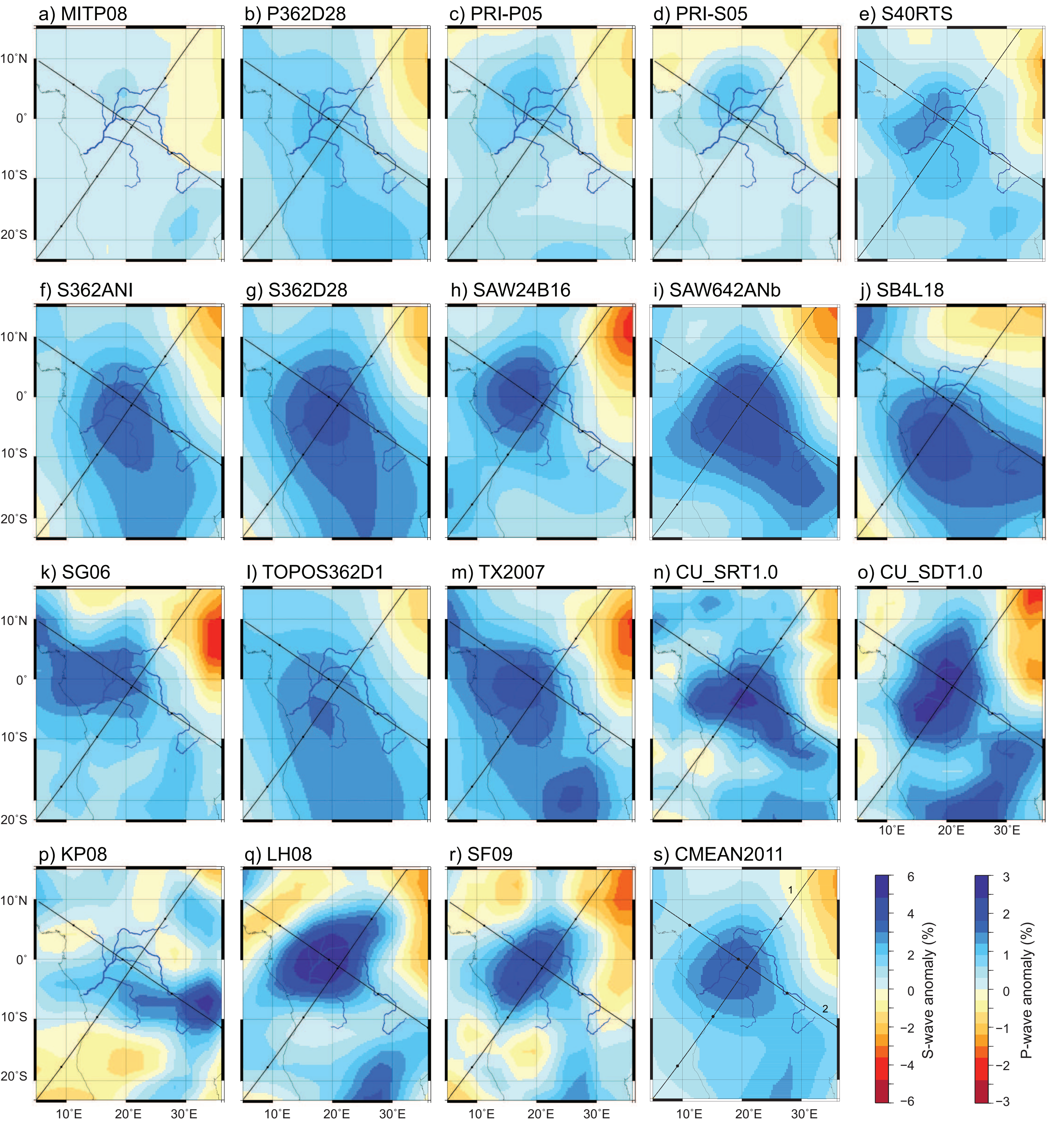
a) MITP08
b) P362D28
c) PRI-P05
d) PRI-S05
e) S40RTS
f) S362ANI
g) S362D28
h) SAW24B16
i) SAW642ANb
j) SB4L18
k) SG06
l) TOPOS362D1
m) TX2007
n) CU_SRT1.0
o) CU_SDT1.0
p) KP08
q) LH08
r) SF09
s) CMEAN2011
10°N
0°
10°S
20°S
10°E
20°E
30°E
1
2
S-wave anomaly (%)
6
4
2
0
−2
−4
−6
P-wave anomaly (%)
3
2
1
0
−1
−2
−3

Figure 11

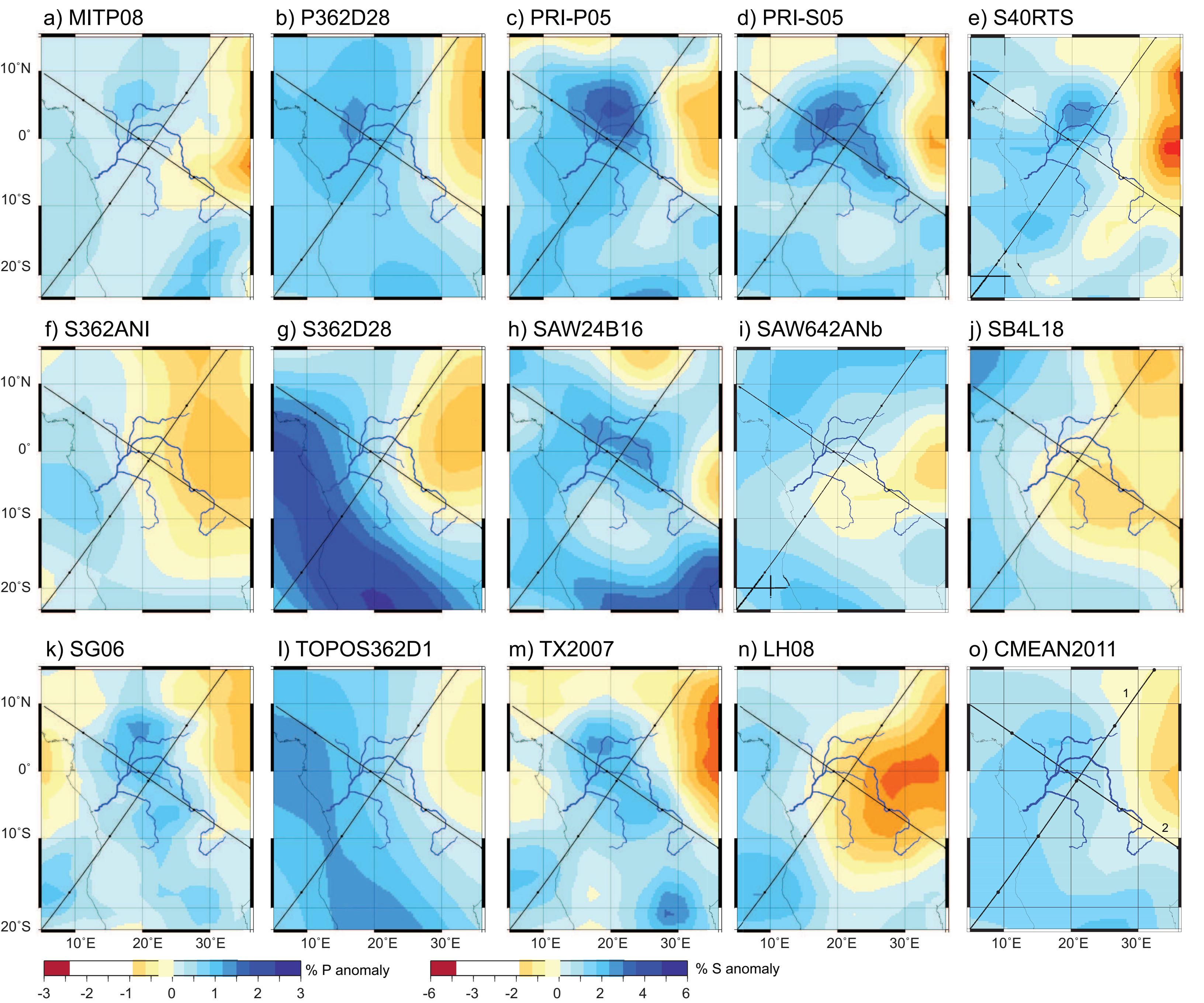

a) MITP08
b) P362D28
c) PRI-P05
d) PRI-S05
e) S40RTS
f) S362ANI
g) S362D28
h) SAW24B16
i) SAW642ANb
j) SB4L18
k) SG06
l) TOPOS362D1
m) TX2007
n) LH08
o) CMEAN2011
10°N
0°
10°S
20°S
10°E
20°E
30°E
1
2
% P anomaly
-3
-2
-1
0
1
2
3
% S anomaly
-6
-3
-2
0
2
4
6

Figure 12

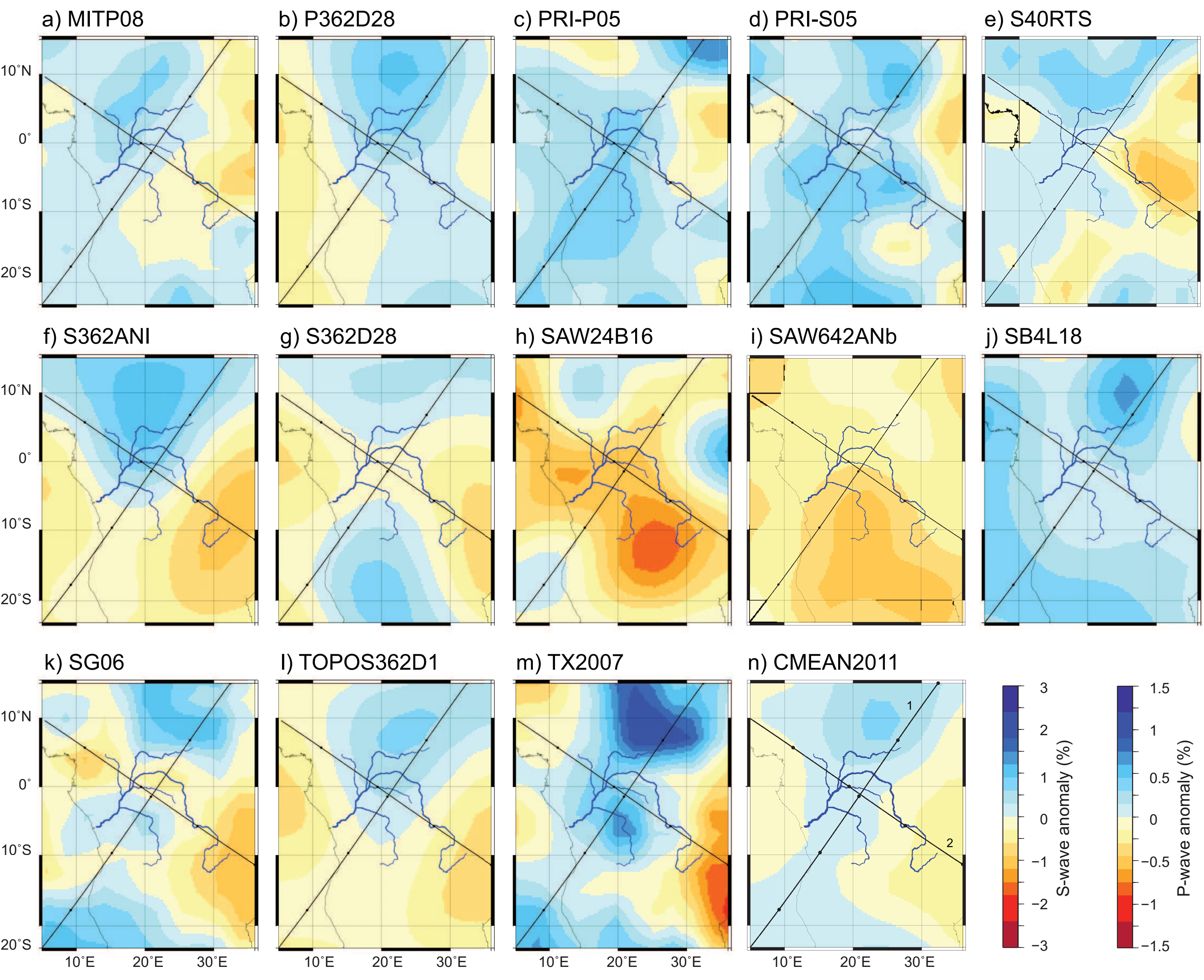
a) MITP08
b) P362D28
c) PRI-P05
d) PRI-S05
e) S40RTS
f) S362ANI
g) S362D28
h) SAW24B16
i) SAW642ANb
j) SB4L18
k) SG06
l) TOPOS362D1
m) TX2007
n) CMEAN2011
10°N
0°
10°S
20°S
10°E
20°E
30°E
1
2
S-wave anomaly (%)
3
2
1
0
−1
−2
−3
P-wave anomaly (%)
1.5
1
0.5
0
−0.5
−1
−1.5

Figure 13

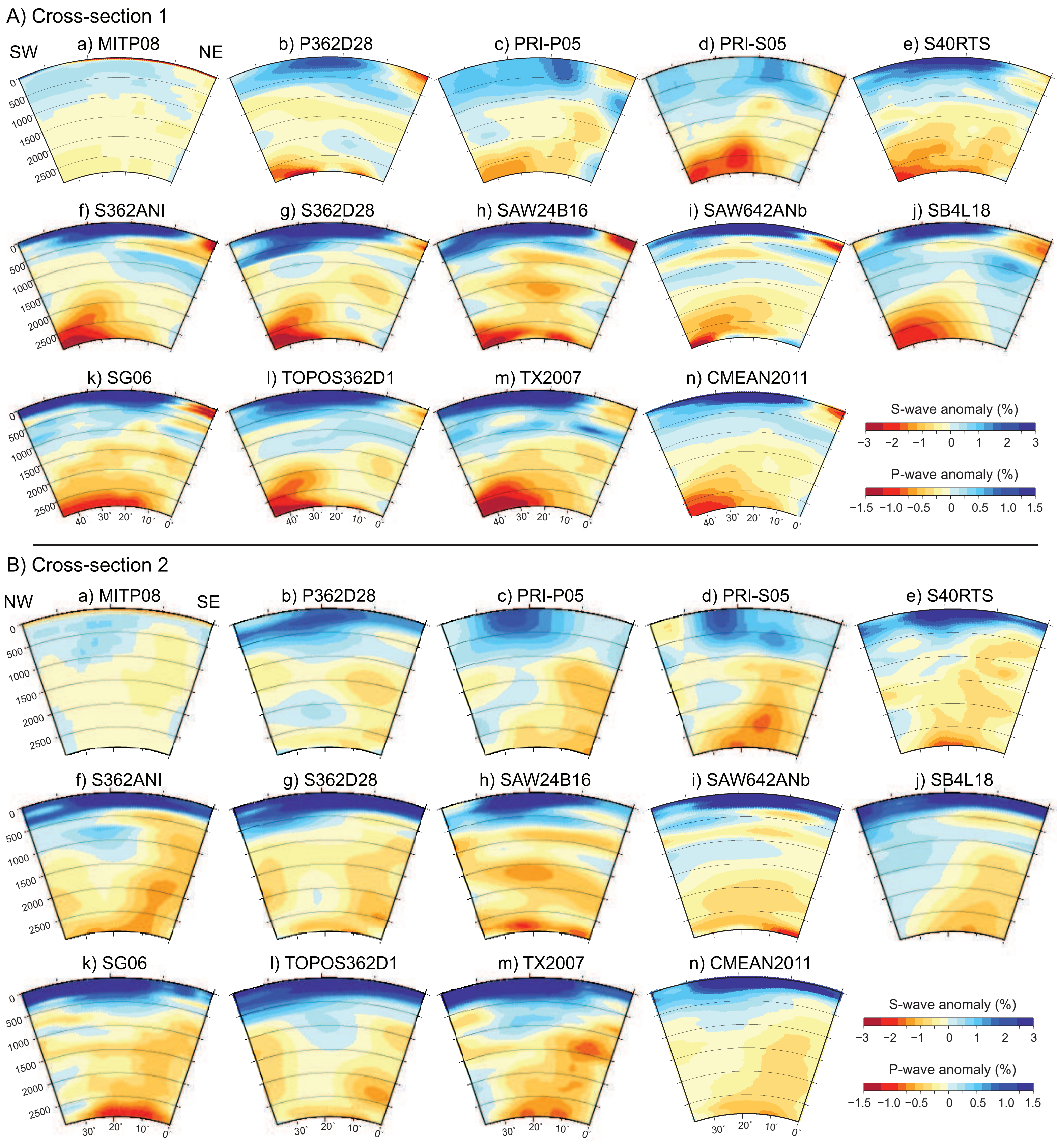

A) Cross-section 1
SW
NE
a) MITP08
b) P362D28
c) PRI-P05
d) PRI-S05
e) S40RTS
f) S362ANI
g) S362D28
h) SAW24B16
i) SAW642ANb
j) SB4L18
k) SG06
l) TOPOS362D1
m) TX2007
n) CMEAN2011
S-wave anomaly (%)
P-wave anomaly (%)
B) Cross-section 2
NW
SE
a) MITP08
b) P362D28
c) PRI-P05
d) PRI-S05
e) S40RTS
f) S362ANI
g) S362D28
h) SAW24B16
i) SAW642ANb
j) SB4L18
k) SG06
l) TOPOS362D1
m) TX2007
n) CMEAN2011
S-wave anomaly (%)
P-wave anomaly (%)